Radar, Passive Microwave, and Lightning Characteristics of Precipitating Systems in the Tropics

E. R. TORACINTA* AND DANIEL J. CECIL+

Department of Atmospheric Sciences, Texas A&M University, College Station, Texas

EDWARD J. ZIPSER AND STEPHEN W. NESBITT

Department of Meteorology, University of Utah, Salt Lake City, Utah

(Manuscript received 20 March 2001, in final form 14 August 2001)

ABSTRACT

The bulk radar reflectivity structures, 85- and 37-GHz brightness temperatures, and lightning characteristics of precipitating systems in tropical Africa, South America, the east Pacific, and west Pacific are documented using data from the Tropical Rainfall Measuring Mission (TRMM) satellite during August, September, and October of 1998. The particular focus is on precipitation features [defined as a contiguous area $\geq$75 km^2 with either a near-surface reflectivity $\geq$20 dB*Z or* an 85-GHz polarization-corrected temperature (PCT) $\leq$ 250 K] with appreciable rainfall, which account for the bulk of the total rainfall and lightning flash density in their respective regions. Systems over the tropical continents typically have greater magnitudes of reflectivity extending to higher altitudes than tropical oceanic systems. This is consistent with the observation of stronger ice scattering signatures (lower 85- and 37-GHz PCT) in the systems over land. However, when normalized by reflectivity heights, tropical continental features consistently have *higher* 85-GHz PCT than tropical oceanic features. It is inferred that greater supercooled water contents aloft in the tropical continental systems contribute to this brightness temperature difference.

Lightning (as detected by the Lightning Imaging Sensor) is much more likely in tropical continental features than tropical oceanic features with similar brightness temperatures or similar reflectivity heights. Vertical profiles of radar reflectivity add additional information to the nonunique lightning–brightness temperature relationships showing that features with lightning tend to have greater magnitudes of reflectivity and smaller decreases of reflectivity with height above the freezing level than systems without detected lightning.

Regional comparisons of the lightning, radar, and microwave signatures of precipitating features show that, over the oceans, the west Pacific has the highest frequency of intense precipitation features (by minimum PCT or maximum reflectivity height). Over land, the intense precipitation features occur more frequently in Africa. These observations are consistent with the relative differences in lightning flash density between the land and ocean regions. The quantitative database of land and ocean features presented here provides a substantial observational framework against which cloud and radiative transfer model results can be tested.

1. Introduction

A considerable effort has been put forth during the last half century to study and understand precipitating systems in the Tropics, which account for two-thirds of the global rainfall and are a major source of latent heat for the atmosphere (Simpson et al. 1986). The spectrum of precipitating cloud types in the Tropics covers a broad range of spatial and temporal scales, ranging from single cumulonimbus clouds to large, long-lived mesoscale convective systems (MCSs), with varying contributions to total tropical rainfall (Mohr et al. 1999). Tropical precipitating systems are also a major component of the global electric circuit with approximately 75% of the global lightning occurring between 30°N and 30°S (Christian et al. 1999). While the charge separation processes leading to lightning are not fully understood it is widely accepted (based on a wealth of laboratory evidence together with in situ observations of thunderstorms) that mixed (liquid and ice) phase cloud microphysics play an essential role. Specifically, noninductive collisions involving millimeter-sized ice (graupel or hail) and smaller ice crystals in the presence of supercooled liquid water at temperatures between 0° and

* Current affiliation: Polar Meteorology Group, Byrd Polar Research Center, The Ohio State University, Columbus, Ohio.

+ Current affiliation: National Space Science and Technology Center, University of Alabama in Huntsville, Huntsville, Alabama.

Corresponding author address: Dr. E. Richard Toracinta, Polar Meteorology Group, Byrd Polar Research Center, The Ohio State University, 108 Scott Hall, 1090 Carmack Rd., Columbus, OH 43210-1002.
E-mail: toracint@polarmet1.mps.ohio-state.edu

−40°C represent the most viable mechanism to explain robust cloud electrification (Reynolds et al. 1957; Takahashi 1978; Jayaratne et al. 1983; Saunders et al. 1991; Williams 1989; and others).

While precipitating cloud systems occur throughout the Tropics, lightning has a strong land bias (Orville and Henderson 1986; Goodman and Christian 1993; Christian 1999; Toracinta and Zipser 2001). This has led many researchers to investigate the microphysical relationships between occurrence or absence of lightning and the structure and environment of tropical convective systems, often with the aid of remote sensing (radar or high-frequency passive microwave) techniques (Williams et al. 1992; Rutledge et al. 1992; Zipser 1994; Petersen et al. 1996; Black and Hallett 1999; Cecil et al. 2002; Cecil and Zipser 2002; Boccippio et al. 2000; Carey and Rutledge 2000; Petersen and Rutledge 2001; Williams et al. 2000; Toracinta and Zipser 2001). Information from radar and passive microwave instruments is useful in this regard because they take advantage of the interaction of microwave energy with liquid and ice phase hydrometeors. Radar reflectivity is strongly related to the size (diameter to the sixth power for Rayleigh scatterers) of the precipitation particles in a sampled volume. Although reflectivity alone is insufficient to distinguish liquid and ice hydrometeors, hydrometeor phase is an important component of reflectivity measurements owing to the difference in the dielectric constants of ice and liquid water, which translates into a nearly 7-dB difference when sampling ice versus liquid phase particles.

For downward looking radiometers, measured brightness temperatures (T_b) are the integrated result of emission and scattering processes that act to modulate upwelling radiation along the optical path to the radiometer. In the remote sensing of precipitating systems the emission sources are primarily cloud liquid water, rain, and melting phase hydrometeors (Wiheit 1986; Mugnai et al. 1990; Vivekanandan et al. 1991). At 37 and 85 GHz, the frequencies used in this and many other studies of convective systems, scattering of upwelling radiation is primarily due to precipitation-sized ice hydrometeors present above the emitting rain layer (Wilheit et al. 1982; Wu and Weinman 1984; Spencer et al. 1989). The resulting reduction of the observed brightness temperatures, termed the ice scattering signatures, is a function of the particle size distribution, bulk density, number concentration, and the geometric depth of the scattering layer (Vivekanandan et al. 1990, 1991). Ice scattering at 85 GHz (3.5-mm wavelength) can be accomplished by relatively small precipitation sized ice (e.g., few hundred microns) and is typically the dominant signal when ice phase precipitation is present, while 37-GHz (8-mm wavelength) ice scattering is attributed to the presence of larger (millimeter sized) graupel or frozen raindrops in convective cores.

Nesbitt et al. (2000) present a census of a large number of tropical precipitating systems, defined using radar and passive microwave data from the Tropical Rainfall Measuring Mission (TRMM) satellite (Simpson et al. 1986; Kummerow et al. 1998), for August, September, and October 1998. In the current study, we make use of the Nesbitt et al. (2000) database and extend their work to examine specific relationships between reflectivity, passive microwave, and lightning characteristics of tropical precipitating systems. A primary objective is to provide a substantial quantitative observational database of these properties, organized in a way that facilitates the evaluation of existing hypotheses regarding microphysical differences between systems with and without detectable lightning. Cecil et al. (2002) and Cecil and Zipser (2002) present a similar quantitative database of tropical cyclones observed by TRMM. Section 2 gives an overview of the TRMM data and the basic technique used to construct the database of precipitating systems. Section 3 presents the combined radar, passive microwave, and lightning characteristics for land and ocean storms along with regional comparisons of storms with and without detectable lightning. The microphysical implications of the land and ocean results are discussed in section 4 and summarized in section 5.

2. Data and methods

a. TRMM satellite, instrumentation, and data

The TRMM satellite was launched in late November 1997 into a circular orbit at approximately 350-km altitude and 35° inclination from the equatorial plane. With this orbital geometry, TRMM precesses through the diurnal cycle at a given geolocation in approximately 47 days. The current study uses data from the TRMM Microwave Imager (TMI; Kummerow et al. 1998), the Precipitation Radar (PR; Kummerow et al. 1998), and the Lightning Imaging Sensor (LIS; Christian 1999).

The PR is a 2-m active phased array radar system operating near 13.8 GHz (approximately 2.2-cm wavelength). The PR scans across a 215-km swath with 80 vertical range bins extending to 20 km above the earth ellipsoid. The vertical and horizontal resolutions are 250 m and 4.3 × 4.3 km^2, respectively, at nadir, while the minimum detectable signal is approximately 17 dBZ at 350-km range. The current study utilizes the attenuation-corrected reflectivity data from the TRMM Science Data and Information System (TSDIS) 2A25 version 4.0 algorithm. (Detailed information about the PR algorithms can be found online at http://tsdis.gsfc.nasa.gov.)

The TMI is a conical scanning multichannel passive microwave radiometer measuring upwelling radiance at 10.65, 19.35, 21.3, 37.0, and 85.5 GHz (85 GHz hereafter) at a 49° angle from nadir. Each TMI frequency is horizontally and vertically polarized except 21.3 GHz, which is vertically polarized. The ground footprints of the 37- and 85-GHz channels are 16 × 9 km^2 and 7 × 5 km^2, respectively, with the major axes oriented along-track. During the time of a full TMI scan, the TRMM

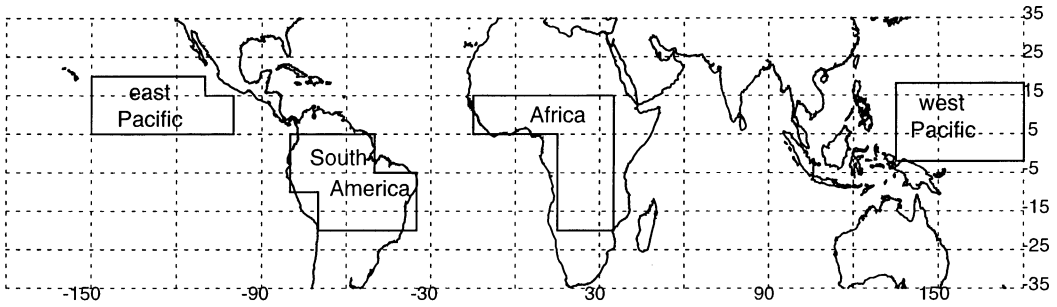

FIG. 1. Map of study regions.

subsatellite point advances approximately 14 km, which results in an alongtrack undersampling at 85 GHz and a slight oversampling at 37 GHz (see Kummerow et al. 1998, Fig. 2). Although the full TMI swath width is 759 km, the current study focuses on data within the 215-km-wide PR swath in order to take advantage of the instrument overlap there.

At TMI frequencies, the ocean surface has a much lower emissivity than land surfaces such that large brightness temperature gradients appear along coastlines. In addition, the emissivity of land surfaces can vary due to the presence of surface water bodies (i.e., lakes) and changes in soil moisture and vegetation. At oblique viewing angles like that used by the TMI, water surfaces are highly polarized. Spencer et al. (1989) make use of the 85-GHz polarization information to derive a polarization-corrected temperature (PCT), which largely eliminates emissivity discontinuities between land and ocean and over varying land surfaces. Their 85-GHz PCT, which is utilized in the current study, is given by

$$\mathrm{PCT}_{85} = 1.8\ T_{85\mathrm{v}} - 0.8\ T_{85\mathrm{h}}, \quad (1)$$

where $T_{85\mathrm{v}}$ and $T_{85\mathrm{h}}$ are the vertically and horizontally polarized 85-GHz brightness temperatures. A similar empirical technique was used, with a one-dimensional plane-parallel radiative transfer model (Kummerow 1993), to derive the following 37-GHz PCT for this study:

$$\mathrm{PCT}_{37} = 2.2\ T_{37\mathrm{v}} - 1.2\ T_{37\mathrm{h}}, \quad (2)$$

where $T_{37\mathrm{v}}$ and $T_{37\mathrm{h}}$ are the vertically and horizontally polarized 37-GHz brightness temperatures, respectively.

The LIS consists of a starting optical imager and onboard electronics designed to detect and record transient optical radiance events associated with lightning. Radiance events that exceed a threshold value above the continuously averaged background are considered lightning candidates. The LIS instrument instantaneous field of view is approximately 600×600 km^2 and the ground resolution is 4 km at nadir. LIS detects total (intracloud and cloud to ground) lightning with typical view times on the order of 80 s. Although LIS validation is still under investigation, the lightning detection efficiency is currently estimated at 70%–90% (Christian 1999; Boccippio et al. 2000); no correction has been applied for the detection efficiency in the present study.

b. Precipitation feature database and study domain

Nesbitt et al. (2000) present an analysis of the distribution and characteristics of discrete precipitation features using TRMM data for two tropical continental (Africa and South America) and tropical oceanic (west Pacific and east Pacific) regions during August–October 1998. These regions, shown in Fig. 1, were chosen to ensure a large sample of tropical continental and tropical oceanic precipitating systems. Petersen and Rutledge (2001) note a distinction between ''isolated oceanic'' and ''coastal oceanic'' convective regimes. The tropical oceanic regions in this study merge those two types of regimes, but are restricted to the deep Tropics where differences between regimes are small. Much of the variability in Petersen and Rutledge's coastal oceanic regimes occurs at higher latitudes. Also, previous studies (e.g., Mohr et al. 1999) have suggested that Amazonian convection seems to have some tropical oceanic characteristics. Petersen and Rutledge (2001) demonstrate that this is a function of the season, with the convection being most intense (most continental) during the transition from the dry to the wet season. This transition season (austral spring) is used in the present study.

The precipitation features are defined using a combination of the PR 2A25 near-surface reflectivity and TMI 85-GHz PCT data, which ensures inclusion of the precipitating area as well as associated ice scattering areas aloft (i.e., anvil) with an optical depth sufficient for significant brightness temperature depressions at 85 GHz. The present study makes use of the Nesbitt et al. (2000) precipitation feature database and a summary of their experimental design is given here.

The PR and TMI data are first matched to a common grid by interpolating the TMI brightness temperatures to the 4.3×4.3 km^2 PR grid using a nearest neighbor technique. With the TMI pixel spacing approximately 14 km in the alongtrack direction, the interpolation typically resulted in two or three PR pixels being matched with the same TMI brightness temperature. Once the PR and TMI fields are combined, the precipitation fea-

TABLE 1. Summary characteristics of precipitation features from Aug, Sep, and Oct 1998.

	Region			
	Africa	South America	West Pacific	East Pacific
Region area ($\times 10^6$ km^2)	12	11	11	8.5
No. of systems	12 788	12 584	28 550	17 317
System density ($\times 10^{-3}$ km^{-2})	1.1	1.1	2.6	2.0
Percent of systems with LIS-detected lightning	15	12	0.3	0.2
90th percentile system size (km^2)	1276	998	536	814
10th percentile minimum 85-GHz PCT (K)	197	212	241	251
Median 30-dB*Z* height (km)	4.5	4.5	3.25	1.5
90th percentile 30-dB*Z* height (km)	9.0	7.75	6.0	5.04

tures are defined as four or more contiguous pixels (~75 km^2) having either a near-surface reflectivity ≥20 dB*Z* *or* an 85-GHz PCT ≤ 250 K. The 20-dB*Z* near-surface reflectivity criterion is sufficiently above the PR minimum detectable signal (~17 dB*Z*) while ensuring that areas of light rainfall are included in the system. The 250-K PCT threshold, which was first used by Mohr and Zipser (1996) to define mesoscale convective systems from Special Sensor Microwave/Imager (SSM/I) 85-GHz data, denotes areas of significant 85-GHz ice scattering.

Surface snow cover can scatter microwave radiation to produce 85-GHz brightness temperatures similar to those associated with precipitating systems (Grody 1991; Ferraro et al. 1994). In the Tropics, this is a concern in high-elevation regions such as the Andes Mountains where permanent or semipermanent snow cover may exist. Actual precipitating areas with 85-GHz PCT below 250 K are not likely to occur without appreciable radar echo at the surface or aloft. Hence, Nesbitt et al. (2000) apply the criteria of near-surface reflectivity or 6-km reflectivity greater than 15 dB*Z* to ensure that snow artifacts are removed from the database.

LIS lightning flash totals and flash densities are computed for each region in order to compare relative differences in lightning occurrence. Lightning flashes are also assigned to individual precipitation features on a spatial coincidence basis and the lightning flash rate is computed for each feature. While most areas of LIS instrument coverage are viewed for approximately 80 s, a small fraction of LIS flashes have view times less than 60 s, which have been filtered from the dataset to ensure more robust flash rate statistics. *An important note regarding LIS lightning*: with typical LIS view times and assuming a 0.75 detection efficiency (Boccippio et al. 2000), the minimum detectable flash rate is approximately 1.0 min^{-1}. As Boccippio et al. (2000) point out, it is not possible with the current dataset to determine the population of storms flashing at rates less than about 1.0 min^{-1} and results using LIS data must be viewed in light of that constraint. Thus, in the following comparisons of systems with and without lightning, *those termed without lightning are understood to have either no flashes or flash rates below the LIS minimum detectable flash rate.*

Our approach to characterizing the precipitation features in this database is to use single value parameters (minimum 85- and 37-GHz PCT, maximum height of threshold reflectivities, and lightning flash rate) for each system. Also, the vertical reflectivity profiles are computed using the maximum reflectivity at each vertical level from anywhere in the system. In any given storm, these values may not be coincident. However, based on theory (Wilheit et al. 1982; Mugnai et al. 1990; Adler et al. 1991; Vivekanandan et al. 1991) and observations (Spencer 1986; Hakkarinen and Adler 1988; Rutledge and MacGorman 1988; Heymsfield and Fulton 1988, 1994; Fulton and Heymsfield 1991; Keighton et al. 1991; Toracinta et al. 1996; Mohr et al. 1996; Petersen et al. 1996, 1999; Carey and Rutledge 2000), including detailed examination of hundreds of individual precipitation features from this dataset, we are making an implicit assumption that the relationships between them are sufficiently robust for describing and comparing the *relative strengths* of the strongest convective events within convective systems and the relationship to lightning.

3. Results

a. General characteristics of land and ocean precipitation features

Table 1 shows that precipitation features occur with greater frequency in the tropical ocean regions than in the tropical land regions even when normalized by the respective region areas. The large majority of features in each of the four regions do not have lightning (as measured by LIS), although the likelihood of a precipitation feature having lightning is more than 40 times greater over land than ocean. The regions are stratified in Table 1 by the 10th percentile minimum 85-GHz PCT, which shows that features with the strongest ice scattering occur in Africa. Features in the east Pacific have the weakest ice scattering, with minimum 85-GHz PCT greater than 250 K in more than 90% of the population. Land systems have much stronger 85-GHz ice scattering with a 30–50-K difference in the 10th percentile minimum PCT. Similarly, tropical land features have deeper 30-dB*Z* reflectivity than those over the tropical oceans

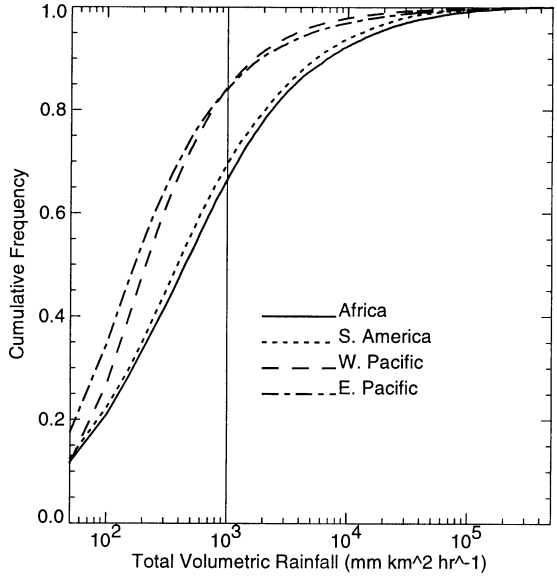

FIG. 2. Cumulative distribution of precipitation features by total volumetric rainfall (mm km^2 h^{-1}) for Africa (solid), South America (dotted), west Pacific (dashed), and east Pacific (dotted–dashed). Volumetric rainfall threshold (10^3 mm km^2 h^{-1}) is indicated (see text).

with African features having the highest 30-dB*Z* echo heights of the four regions.

Significant land–ocean differences also occur in the distributions of precipitation feature volumetric rainfall, which are shown in Fig. 2. The two land and the two ocean regions have very similar rainfall distributions with the tropical oceanic features producing lower rainfall totals than tropical continental features. The bulk of the total volumetric rainfall over land and ocean is contributed by a small fraction of precipitating systems, as early researchers have noted (e.g., Riehl 1954) and recent satellite-based studies confirm (Mohr et al. 1999; Nesbitt et al. 2000). In order to concentrate on systems producing significant rainfall, the population of features was reduced to those exceeding an arbitrary volumetric rainfall threshold (10^3 mm km^2 h^{-1}). Applying the threshold reduces the land and ocean populations by approximately 67% and 84%, respectively. Table 2 compares summary characteristics for features that do and do not exceed the rainfall threshold. As select case studies of tropical convection indicate (e.g., Carey and Rutledge 2000), the relatively small fraction of systems that produces most of the rainfall also produces nearly all of the lightning. In contrast, the bulk of the subthreshold precipitation features in each region are shallow precipitating systems (by 30-dB*Z* echo height), which contribute little to LIS lightning flash totals and have little or no 85-GHz ice scattering (at TMI resolution). Therefore, these systems will be excluded from further analysis and unless stated otherwise, *subsequent use of the term precipitation feature will refer only to the subset of systems that exceed the rainfall threshold.*

b. PR reflectivity and TMI brightness temperature signatures

A simple but useful method to describe and compare the vertical reflectivity structures of tropical continental and tropical oceanic precipitation features is with the maximum heights of threshold reflectivity values. This method is used in Fig. 3a, which shows the frequency distributions of land and ocean precipitation features according to their maximum 20- and 30-dB*Z* echo-top heights. Nearly half (45%) of the tropical oceanic precipitation features and roughly one-third of the tropical continental features have maximum 20-dB*Z* echo-top heights between 6 and 10 km and maximum 30-dB*Z* echo-top heights ranging from 5 to 7 km. The deepest 30-dB*Z* heights in continental features extend to greater extremes than those in oceanic features. In fact, inspection of the reflectivity height distributions shows that land features typically have deeper 30-dB*Z* echoes than ocean features with similar 20-dB*Z* echo-top heights. A quantitative example of this is shown in Fig. 4a, which compares the frequency distributions of 30- and 40-dB*Z* heights for the subset of land and ocean precipitation features with maximum 20-dB*Z* heights from 13 to 14 km. For features with the same 20-dB*Z* echo-top heights, those over land have modal 30-dB*Z* echo-top heights that are 3 km higher than those over the oceans.

Tropical continental features have 40-dB*Z* reflectivities extending to much higher extremes ($>$15 km) than those in the tropical ocean features (Fig. 3b). In sharp contrast, the 40-dB*Z* echo-top heights in tropical oceanic

TABLE 2. Summary characteristics of precipitation features that do not meet the total volumetric rainfall threshold (10^3 mm km^2 h^{-1}). Values in parentheses correspond to precipitation features that meet the total volumetric rainfall threshold.

	Region			
	Africa	South America	West Pacific	East Pacific
No. of systems	8380 (4408)	8632 (3952)	23 918 (4632)	14 489 (2828)
Median minimum 85-GHz PCT (K)	277 (237)	278 (244)	284 (243)	283 (254)
Median maximum 30-dB*Z* height (km)	4.25 (7.25)	4.0 (6.5)	3.0 (6.0)	1.25 (5.25)
No. with LIS lightning	99 (1795)	86 (1393)	6 (87)	2 (24)
Percent of total LIS flashes	1 (99)	1 (99)	2 (98)	3 (97)
Percent of total volumetric rainfall	5 (95)	6 (94)	16 (84)	10 (90)

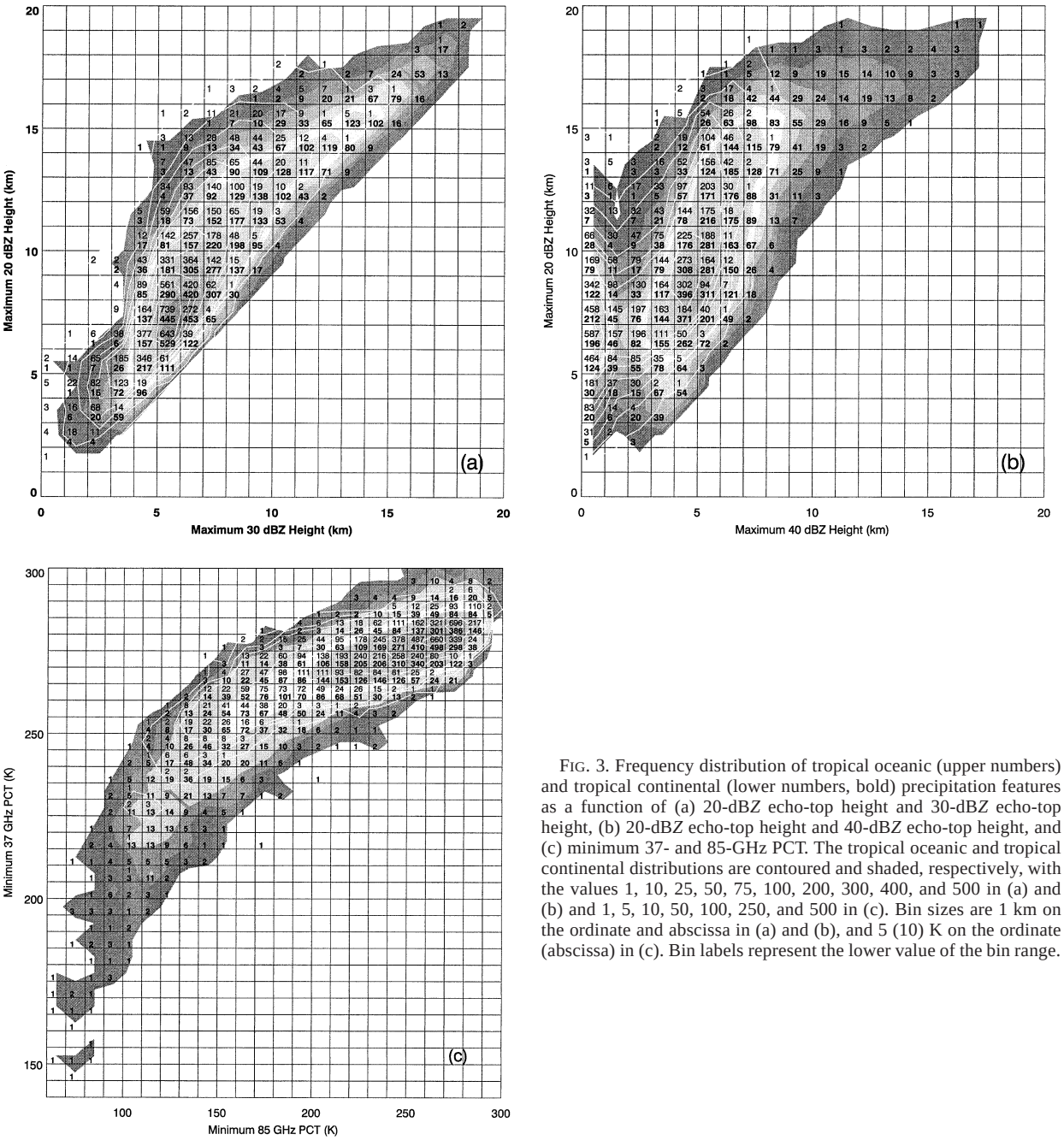

FIG. 3. Frequency distribution of tropical oceanic (upper numbers) and tropical continental (lower numbers, bold) precipitation features as a function of (a) 20-dBZ echo-top height and 30-dBZ echo-top height, (b) 20-dBZ echo-top height and 40-dBZ echo-top height, and (c) minimum 37- and 85-GHz PCT. The tropical oceanic and tropical continental distributions are contoured and shaded, respectively, with the values 1, 10, 25, 50, 75, 100, 200, 300, 400, and 500 in (a) and (b) and 1, 5, 10, 50, 100, 250, and 500 in (c). Bin sizes are 1 km on the ordinate and abscissa in (a) and (b), and 5 (10) K on the ordinate (abscissa) in (c). Bin labels represent the lower value of the bin range.

features are largely confined to below 7 km with nearly one-third of the ocean systems having no 40-dBZ echo. For the fixed 13–14-km 20-dBZ echo-top height (Fig. 4a), the modal 40-dBZ heights in tropical continental and tropical oceanic features differ by 1 km.

The frequency distributions of the tropical continental and tropical oceanic features by their minimum 37- and minimum 85-GHz PCT (Fig. 3c) show two clean results. First, land features dominate the low brightness temperature extremes. For instance, there are very few oceanic features with 85-GHz PCT $<$ 150 K and 37-GHz PCT $<$ 240 K, where strong ice scattering is occurring at both frequencies. Second, the highest frequency of land and ocean features occurs at the warm end of the T_b parameter space (37-GHz PCT $>$ 275 K and 85-GHz PCT $>$ 250 K). This is indicative of minimal 85-GHz ice scattering, consistent with the reflectivity profiles not extending far above the freezing level (not shown).

Figure 3c also indicates that when the features are normalized by the 85-GHz ice scattering signature, particularly where appreciable 85-GHz ice scattering oc-

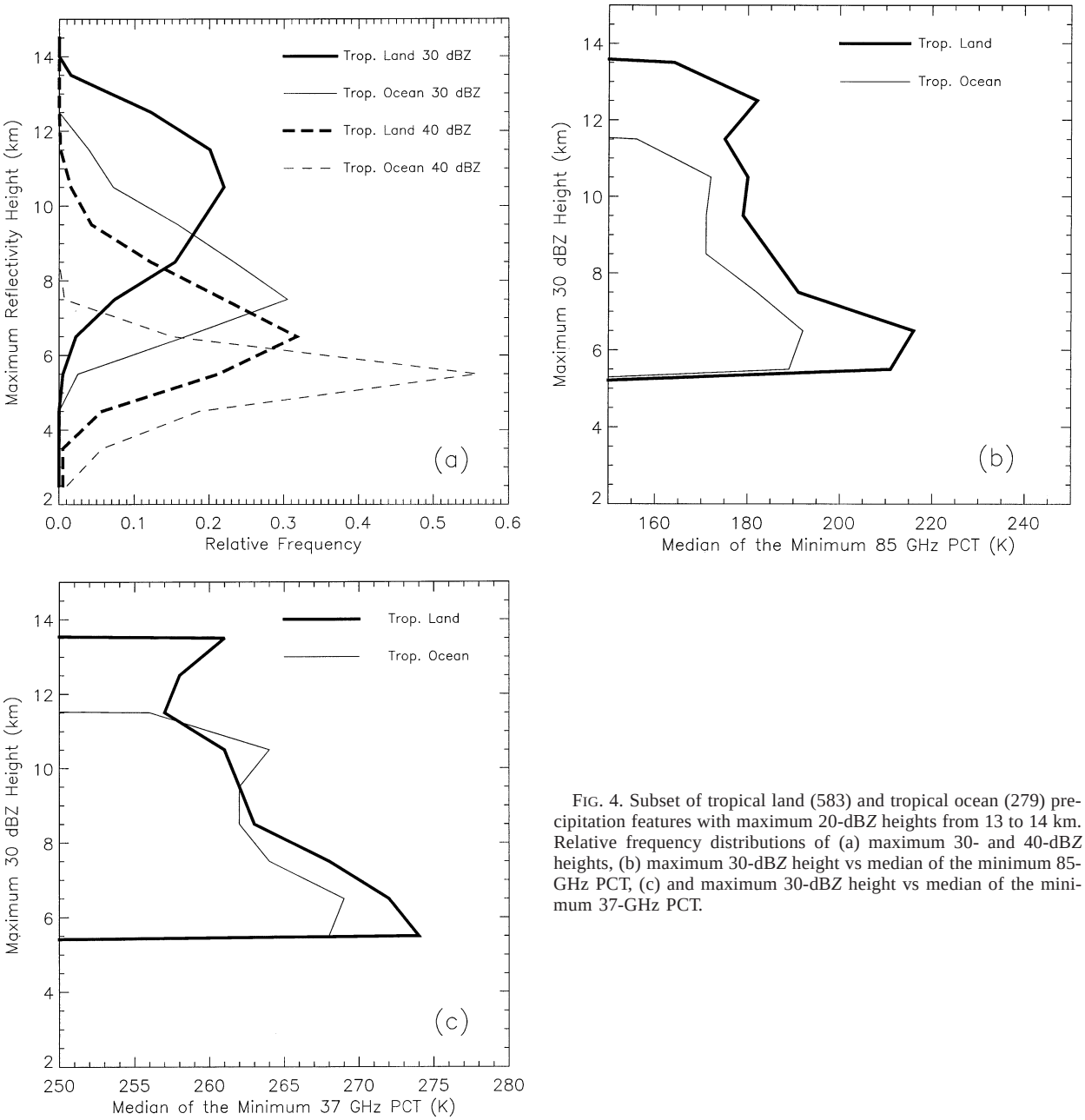

FIG. 4. Subset of tropical land (583) and tropical ocean (279) precipitation features with maximum 20-dBZ heights from 13 to 14 km. Relative frequency distributions of (a) maximum 30- and 40-dBZ heights, (b) maximum 30-dBZ height vs median of the minimum 85-GHz PCT, (c) and maximum 30-dBZ height vs median of the minimum 37-GHz PCT.

curs (PCT $<$ 250), tropical continental features tend to have colder 37-GHz PCT than their oceanic counterparts. For example, tropical continental and tropical oceanic features with minimum 85-GHz PCT between 200 and 210 K have modal 37-GHz PCTs that differ by 4 K. The difference increases to around 6 K as the 85-GHz PCT decreases. Along with the observed deeper 30- and 40-dBZ reflectivity in tropical continental features, this trend suggests the presence of larger (or more) graupel or hail in the tropical continental systems than in systems over the tropical oceans.

As the 37-GHz PCTs decrease below about 255 K in Fig. 3c, the tropical oceanic features are confined to a lower, more narrow range of 85-GHz PCTs than the corresponding tropical continental features. An example is the subset of tropical land and ocean systems with minimum 37-GHz PCT from 245 to 250 K. These have similar modal 85-GHz PCT (140–150 K), but *only the tropical land systems* have minimum 85-GHz PCT extending to much higher values above 170 K. This may be due to the presence of greater supercooled cloud liquid water contents aloft in the land systems, which when present in the ice layer, can act as an emission source to reduce the effects of 85-GHz ice

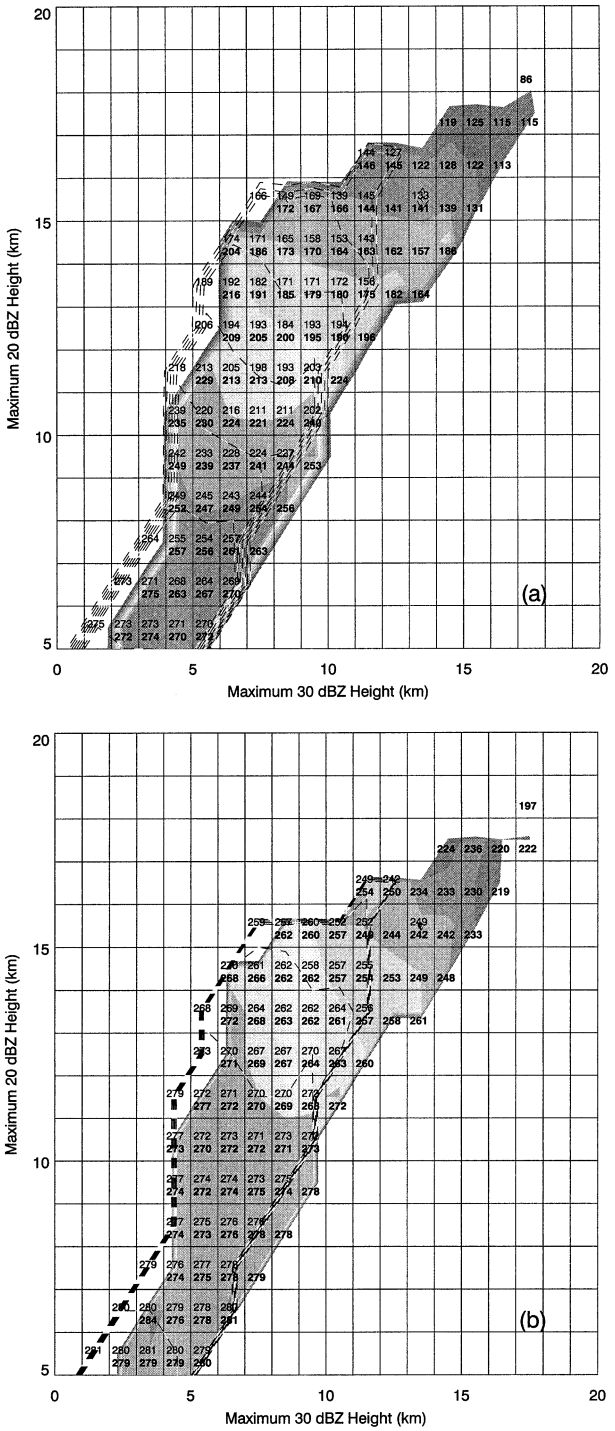

FIG. 5. (a) Median of the minimum 85-GHz PCT and (b) median of the minimum 37-GHz PCT for tropical oceanic (upper numbers) and tropical continental (lower numbers, bold) precipitation features. The tropical oceanic and tropical continental distributions are contoured and shaded, respectively, with intervals of 25 K beginning at 100 K in (a) and 10 K beginning at 220 K in (b). Bin sizes are 1 km for the ordinate (maximum 20-dB*Z* height) and abscissa (maximum 30-dB*Z* height). Bin labels represent the lower value of the bin range. Bins containing fewer than five precipitation features (from Fig. 3a) are not plotted.

scattering and increase the observed T_b (Adler et al. 1991; Vivekanandan et al. 1991; Smith et al. 1992; Seo 2000).

To more closely examine the reflectivity and brightness temperature relationships, Fig. 5a compares the median minimum 85-GHz PCT for continental and oceanic systems as a function of their maximum 20- and 30-dB*Z* echo-top heights. The median 85-GHz PCTs tend to decrease with increasing 20- and 30-dB*Z* heights, consistent with increased 85-GHz ice scattering with increasing optical depth. The trend is similar with the median 37-GHz PCT shown in Fig. 5b, although the brightness temperature decrease is more gradual since the 37-GHz ice scattering requires the presence of larger graupel or hail particles than at 85 GHz.

Figure 5a also shows that for tropical land and ocean features with the *same reflectivity heights*, the median 85-GHz PCTs are substantially *higher* for tropical continental than corresponding tropical oceanic values. An example is shown in Fig. 4b for features with 13–14-km 20-dB*Z* heights where, at any given 30-dB*Z* height, the 85-GHz PCT in continental features is 10–25 K warmer than in the tropical oceanic features. The 37-GHz PCT difference is much smaller than at the higher frequency with less consistency between tropical land and ocean (Fig. 4c). This may be due in part to nonuniform beamfilling effects at 37 GHz, which has a footprint four times larger than at 85 GHz and is therefore not as effective in resolving small ice scattering cores. Another factor could be the presence of greater supercooled cloud liquid water contents in the tropical continental systems relative to the tropical oceanic systems. The emission from supercooled cloud liquid water is greater at higher microwave frequencies (Adler et al. 1991) and, thus, could contribute to the land–ocean difference at 85 GHz (Fig. 4b) with little or no effect at 37 GHz (Fig. 4c).

Figures 6a and 6b show the distributions of median minimum 85-GHz PCT and minimum 37-GHz PCT, respectively, for tropical continental and tropical oceanic features as a function of their maximum 20- and 40-dB*Z* echo-top heights. Among the tropical oceanic features, for a given 20-dB*Z* height the median 85-GHz T_b values decrease as the 40-dB*Z* height increases indicating greater ice scattering with increasing optical depth. The trend is similar at 37 GHz (Fig. 6b) with the lowest median PCT (247 K) occurring with the deepest ocean 20- and 40-dB*Z* reflectivities. For tropical continental features, the median 85-GHz PCTs tend to decrease with increasing 40-dB*Z* height to 5–7 km and then show a slight increase as the 40-dB*Z* heights increase toward the extremes. This 85-GHz T_b increase might be related to microwave emission due to the amount and/or vertical distribution of supercooled cloud liquid water aloft in vigorous tropical continental convective storms with deep 40-dB*Z* reflectivity.

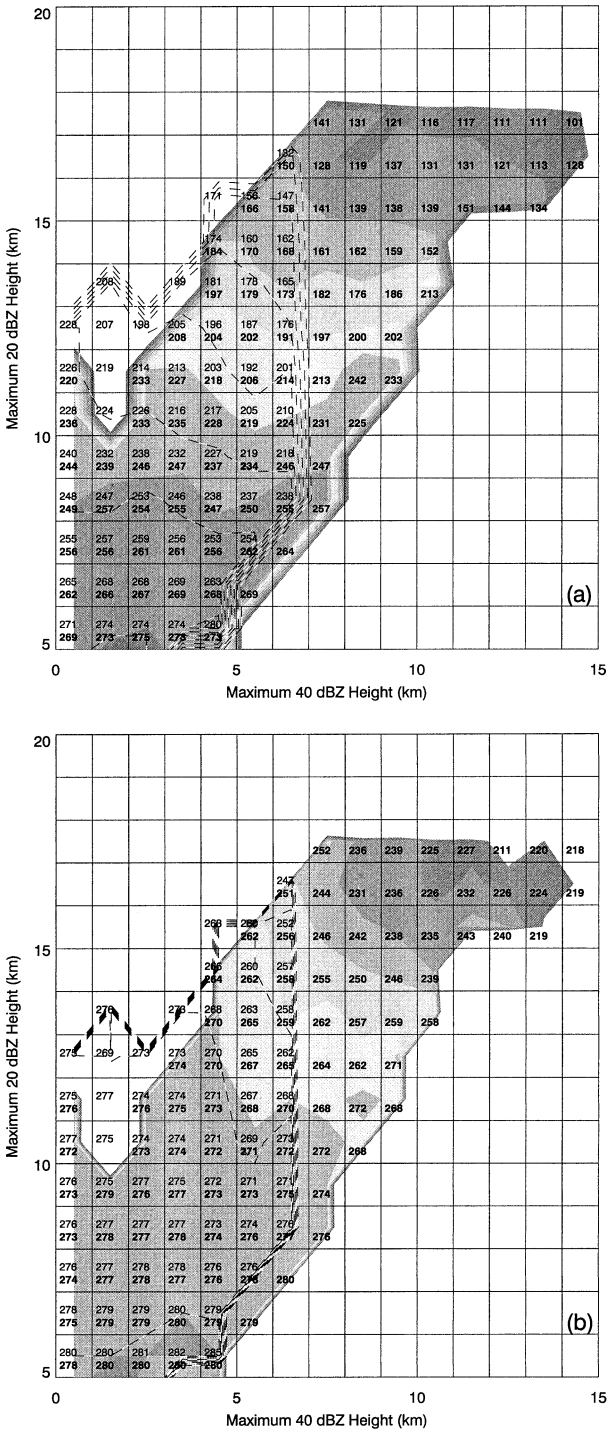

FIG. 6. (a) Median of the minimum 85-GHz PCT and (b) median of the minimum 37-GHz PCT for tropical oceanic (upper numbers) and tropical continental (lower numbers, bold) precipitation features. The tropical oceanic and tropical continental distributions are contoured and shaded, respectively, with intervals of 25 K beginning at 100 K in (a) and 10 K beginning at 220 K in (b). Bin sizes are 1 km for the ordinate (maximum 20-dBZ height) and abscissa (maximum 40-dBZ height). Bin labels represent the lower value of the bin range. Bins containing fewer than five precipitation features (from Fig. 3a) are not plotted.

c. Characteristics of features with and without LIS lightning

The geographic distributions of precipitation features with and without LIS lightning for August–October 1998 are shown in Figs. 7a and 7b, respectively, with summary statistics in Table 3. Of the four regions, the east Pacific has the lowest raw count and spatial density of features, which are largely concentrated along the intertropical convergence zone (ITCZ) around 10°N. The low spatial density is due to the infrequent occurrence of storms over the northern portion of the region (15°–20°N), which is characterized by cooler sea surface temperatures than the southern portion of the region. The spatial density of systems over the rainy portion of the east Pacific (ITCZ) is greater than either of the tropical continental regions. However, a very small fraction (~1%) of east Pacific features have detectable lightning resulting in a low regional flash density. The west Pacific contains the largest raw count and spatial density of features of the four regions. These are also locally concentrated along the ITCZ (~7°N), along with a significant concentration extending northward to 15°N and in the southwestern portion of the region toward New Guinea. Precipitation features without LIS lightning also dominate the west Pacific, accounting for 98% of the systems in the region.

Boccippio et al. (2000) suggest that the greater spatial density of lightning producing storms over tropical land compared to tropical oceans is consistent with more intense, smaller-scale circulations occurring over land. The authors wonder if the spatial densities of storms defined independently of lightning (such as the precipitation features) have a similar land–ocean difference. This is not the case, as the spatial density of precipitation features is greatest in the tropical oceanic ITCZ.

In both tropical land regions the fraction of features with LIS lightning is more than an order of magnitude greater than over the tropical ocean regions; 41% of the features in Africa and 35% of those in South America have detectable lightning (Table 3). Africa contains by far the highest total lightning count and flash density of the four regions. Figure 7a indicates that the lightning systems over Africa have a fairly uniform distribution across the sub-Sahara (5°–15°N) with a slightly higher concentration of lightning features in the central portion of the continent (5°–10°S), and relatively few systems in the southeastern portion of the region. With the exception of southeastern Africa, features without LIS lightning are generally found throughout the region with numerous systems along the western coast (near 5°N, 10°W) and across the sub-Sahara to the central portion of the continent. In South America during this season, systems with lightning are distributed fairly uniformly with the exception of northeastern Brazil (near 5°S, 40°W) and the eastern Brazilian coast. Features without LIS lightning generally increase in frequency of occurrence from southeast to northwest with a small number

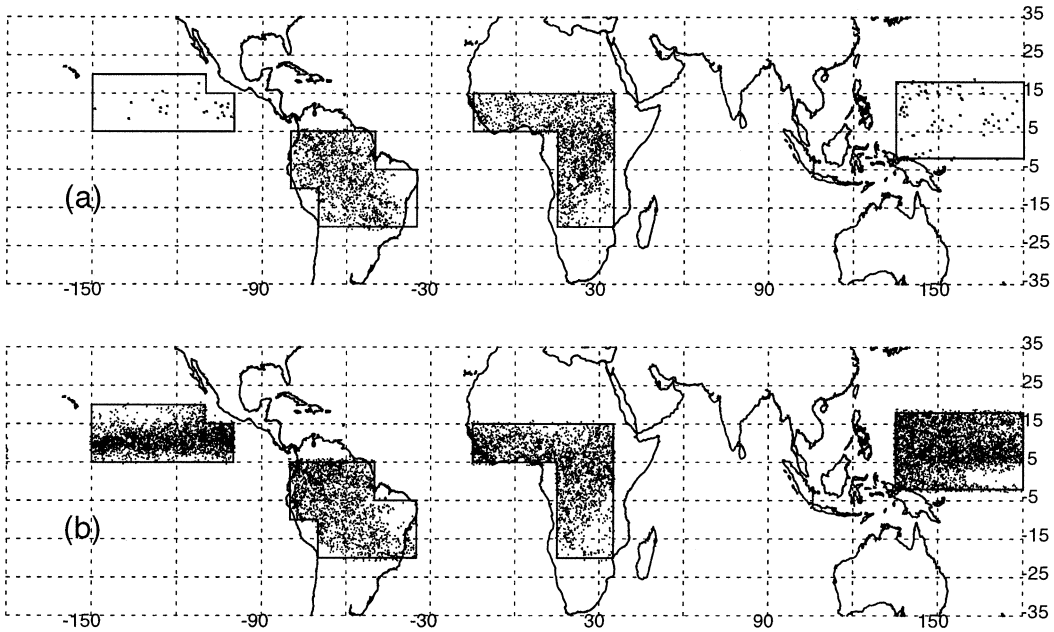

FIG. 7. Geographic locations of precipitation features (a) with and (b) without LIS-detected lightning.

of systems along and off the eastern Brazilian coast and few systems in northeastern Brazil.

While the tropical land and ocean spatial densities of precipitation features given in Table 3 are very similar, the tropical land–ocean differences in the frequency of features with LIS lightning, and thus total regional lightning counts, are quite large. Quantitatively, when normalized by the area of each region, the ratio of tropical continental to tropical oceanic precipitation feature occurrence is roughly 0.95, yet the probability of a lightning system differs by a factor of 25. In addition, the tropical continental flash densities range from a factor of 50 to two orders of magnitude greater than the corresponding tropical oceanic flash densities.

Figure 8 presents relative frequency distributions of African (contoured) and South American (shaded) precipitation features according to their radar reflectivity and microwave brightness temperature characteristics. The left and right panels compare features with and without LIS-detected lightning, respectively. Figures 8a and 8b indicate that the features with and without lightning in Africa and South America are similarly distributed in much of the brightness temperature parameter space. Africa tends to have a greater occurrence of lightning features at the lower brightness temperature extremes (85-GHz PCT $<$ 120 K; 37-GHz PCT $<$ 220 K) than South America. The majority (57%) of African and South American features without LIS lightning have minimum 85-GHz PCT $>$ 250 K and minimum 37-GHz PCT $>$ 270 K. There is, however, considerable overlap in the brightness temperature parameter space between systems with and without detected lightning.

African and South American lightning features have very similar maximum 20- and 30-dB*Z* echo-top heights with 30-dB*Z* echo-top heights reaching at least 5 km in both regions for lightning to occur (Fig. 8c). However, Africa has a greater fraction of lightning features with deep ($>$8 km) 40-dB*Z* echoes than South America (Fig. 8e). Of the systems without LIS lightning, the maximum 20- and 30-dB*Z* echo tops reach similar height extremes for both Africa and South America (Fig. 8d), although African systems have slightly deeper 30-dB*Z* reflectivity for a given 20-dB*Z* height above about 7 km than those in South America. A similar though less pronounced trend occurs with 40-dB*Z* echo-top heights among the systems without detected lightning (Fig. 8f). Again,

TABLE 3. Summary of precipitation features and LIS lightning statistics.

	Region			
	Africa	South America	West Pacific	East Pacific
No. of systems	4408	3952	4632	2828
Spatial system density ($\times 10^{-4}$ km^{-2})	3.7	3.6	4.2	3.3
Total LIS flashes	22 594	13 110	244	77
Spatial flash density ($\times 10^{-5}$ km^{-2})	188	119	2.2	0.9
Percent of systems with lightning	41	35	2	1

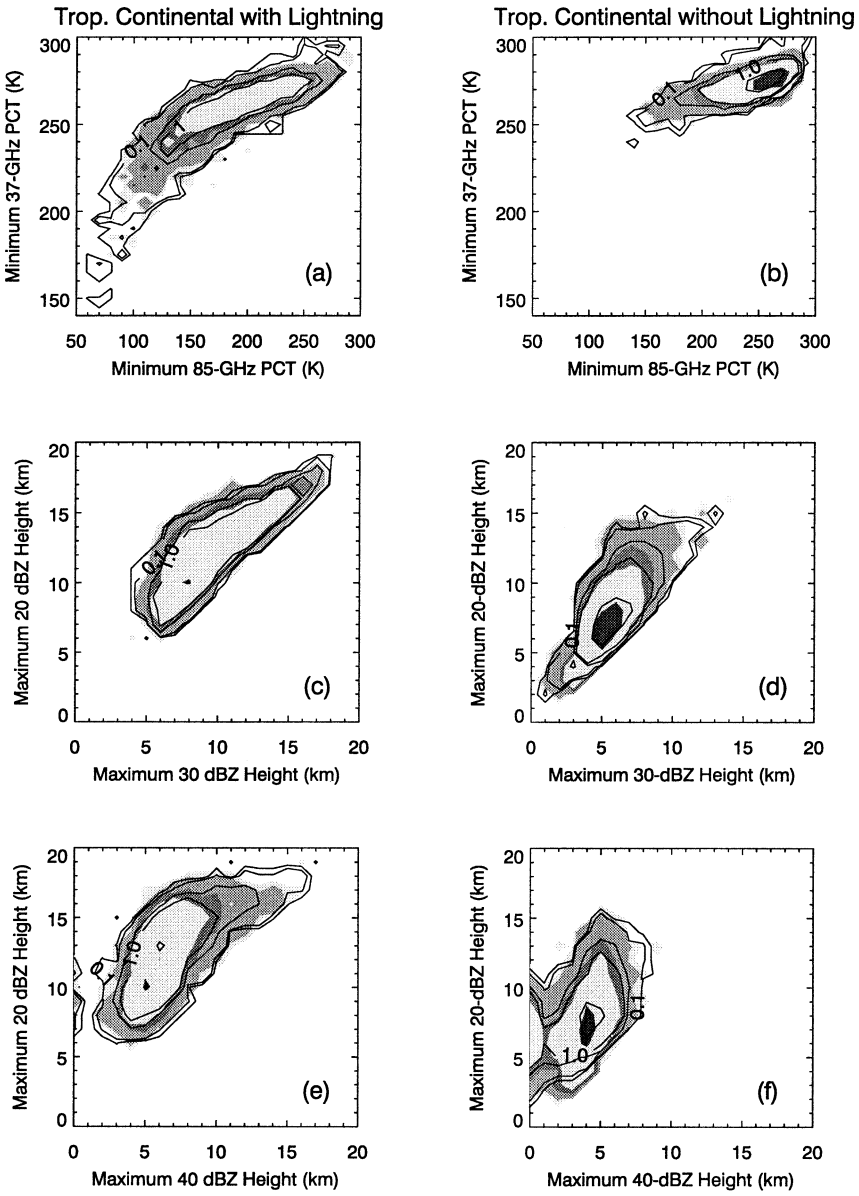

FIG. 8. Relative frequency distribution of precipitation features over Africa (contoured) and South America (shaded). Features with (without) LIS-detected lightning are in the left (right) panels. Contour and shading values are 0.05%, 0.1%, 0.5%, 1%, 5%, and 10%. Bin sizes are 5 (10) K for the ordinate (abscissa) in (a) and (b), and 1 km for the ordinate and abscissa in (c)–(f). Bin labels represent the lower value of the bin range. Sample sizes for African features with (without) LIS lightning are 1795 (2613); sample sizes for South American features with (without) LIS lightning are 1393 (2559).

there is considerable overlap in the reflectivity parameter space between features with and without LIS lightning (cf. Figs. 8c,d). For instance, approximately the same fractions (78%) of tropical continental features with and without lightning have 20-dBZ echo-top heights from 6 to 15 km and 30-dBZ heights ranging from 5 to 14 km. It is likely that at least some of the overlap is due to the LIS minimum detectable flash rate ($\sim$1.0 min^{-1}) constraint.

The relative frequency distributions of west Pacific and east Pacific features with and without LIS lightning are shown in Fig. 9. The east Pacific lightning features are indicated by plus signs due to the small sample size. The majority of east and west Pacific lightning features occupy similar portions of the brightness temperature parameter space (Fig. 9a), although a small fraction of west Pacific lightning features occur at lower T_b extremes. The obvious differences between tropical oceanic and tropical continental systems with lightning are that systems over land occupy broader brightness tem-

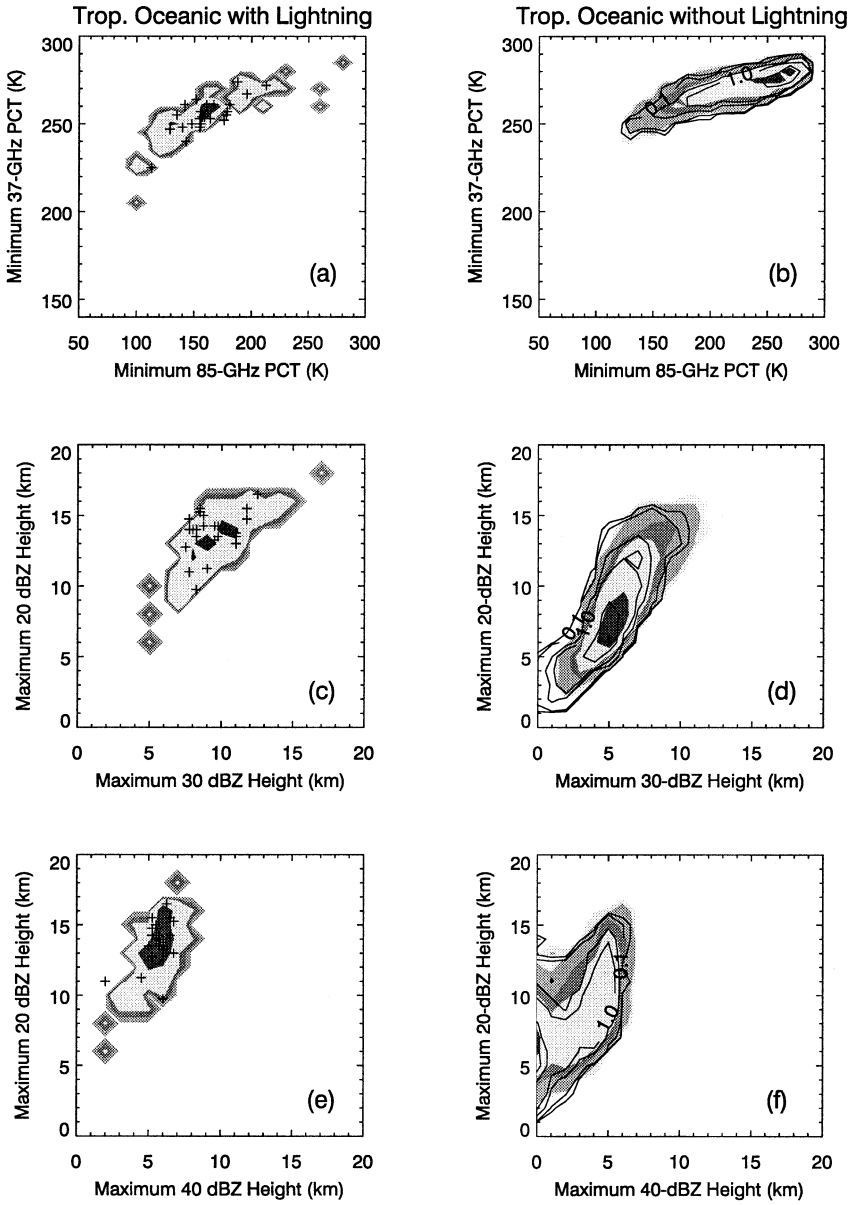

FIG. 9. Relative frequency distribution of precipitation features over west Pacific (contoured) and east Pacific (shaded). Features with (without) lightning are in the left (right) panels. Contour and shading values are 0.05%, 0.1%, 0.5%, 1%, 5%, and 10%. Bin sizes are 5 (10) K for the ordinate (abscissa) in (a) and (b), and 1 km for the ordinate and abscissa in (c)–(f). Bin labels represent the lower value of the bin range. Sample size for west Pacific with (without) LIS lightning is 87 (4545); sample size for east Pacific with (without) LIS lightning is 24 (2804). East Pacific precipitation features with lightning are represented by plus signs due to the small sample size.

perature ranges and attain a greater degree of ice scattering (lower 85- and 37-GHz PCTs) than their tropical oceanic counterparts (cf. Fig. 8a).

The east and west Pacific features without LIS-detected lightning have nearly identical brightness temperature distributions (Fig. 9b). A comparison with Fig. 8b shows that tropical continental and tropical oceanic features without LIS lightning have similar brightness temperature characteristics with the tropical oceanic features skewed slightly toward colder brightness temperatures relative to those over land.

With little exception, tropical oceanic features with and without LIS lightning have similar 20-dBZ echo tops, extending to 16–17 km (Figs. 9c,d). This is a different relationship than among the tropical continental features where features with and without lightning are

distinguished by a 3-km difference in the 20-dB*Z* echo-top height extremes (see Figs. 8c,d). A slightly higher 30-dB*Z* echo (6 km) is required for detectable lightning over the tropical oceans compared with systems over land. West Pacific systems without LIS lightning tend to have deeper 30-dB*Z* reflectivity for a given 20-dB*Z* height than those in the east Pacific (Fig. 9d). East and west Pacific lightning features generally have 40-dB*Z* echo-top heights below 7 km (Fig. 9e), significantly lower than the tropical continental lightning features (see Fig. 8e). Among the tropical oceanic features without LIS lightning (Fig. 9f), the east Pacific generally has shallower 40-dB*Z* reflectivity as well as the majority of tropical ocean features containing no 40-dB*Z* echo.

d. Probability of LIS lightning for tropical land and ocean features

Figure 10a indicates that the LIS-detected lightning probabilities for tropical continental features are nonzero in *virtually every part* of the 85- and 37-GHz brightness temperature parameter space. The lightning probabilities increase rapidly from around 10%–15% for 85-GHz PCT $>$ 250 K to greater than 50% for 85-GHz PCT around 200 K, and 80%–100% for 85-GHz PCT $<$ 170 K. Also, the lightning probabilities appear more sensitive to changes in 37-GHz PCT than 85-GHz PCT. For example, for features with 85-GHz PCTs between 210 and 220 K, the lightning probabilities increase from 29% to 91% as the 37-GHz PCT decrease from about 280 to 255 K. For a fixed 37-GHz PCT, say 260–265 K, the LIS lightning probabilities show a similar increase, but for 85-GHz PCTs there is a decrease from 240 to 140 K. This is consistent with the difference in Mie scattering effects at these two frequencies. At 37 GHz, the wavelength ($\sim$8 mm) is more than twice that at 85 GHz such that the ice scattering response at 37 GHz requires larger graupel or hail particles than at 85 GHz.

The LIS-detected lightning probabilities for tropical oceanic features in much of the brightness temperature parameter space are near zero. Lightning probabilities reach 10% or greater only for features with minimum 85-GHz PCT $<$ 180 K and minimum 37-GHz PCT $<$ 265 K. The greatest tropical oceanic lightning probability (50%) occurs near the tropical oceanic minimum T_b extremes. A comparison of tropical continental and oceanic lightning probabilities shows the striking result that tropical land and ocean systems with *very similar* 85- and 37-GHz signatures have *very different* lightning probabilities. The differences are typically an order of magnitude or larger in regions of the brightness temperature parameter space (150 K $<$ 85-GHz PCT $<$ 250 K; 250 K $<$ 37-GHz PCT $<$ 280 K) containing similar sample sizes of tropical continental and tropical oceanic features.

Figure 10b shows that the lightning probabilities for tropical continental features are 10% or greater when

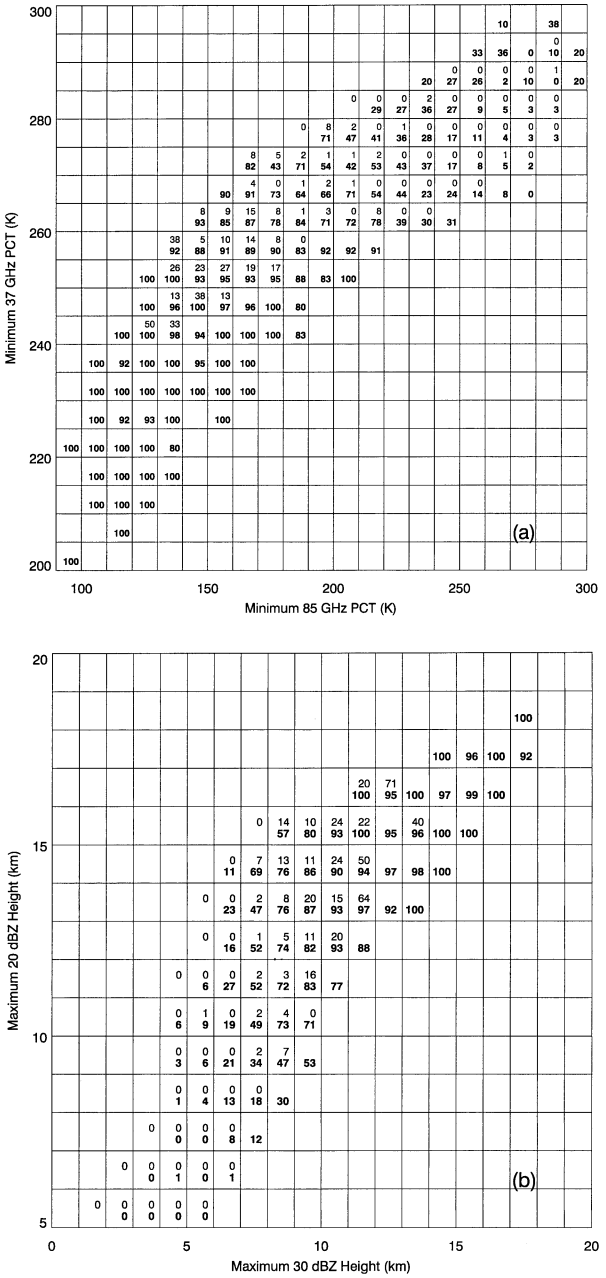

FIG. 10. Fraction of tropical oceanic (upper numbers) and tropical continental (lower numbers, bold) precipitation features with LIS-detected lightning as a function of (a) minimum 37-GHz PCT and minimum 85-GHz PCT and (b) maximum 20-dB*Z* echo-top height and maximum 30-dB*Z* echo-top height. Bin sizes are 5 (10) K on the ordinate (abscissa) in (a) and 1 km on the ordinate and abscissa in (b). Bin labels represent the lower value of the bin range. Bins containing fewer than five precipitation features (from Figs. 3a and 3c) are not plotted.

the 20-dB*Z* echo-top heights exceed 7 or 8 km and the 30-dB*Z* echo-top heights are at least 6 km. The vast majority ($>$80%) of tropical continental features with deep ($>$12 km) 20-dB*Z* echoes and deep ($>$9 km) 30-dB*Z* echoes have LIS lightning. The lightning proba-

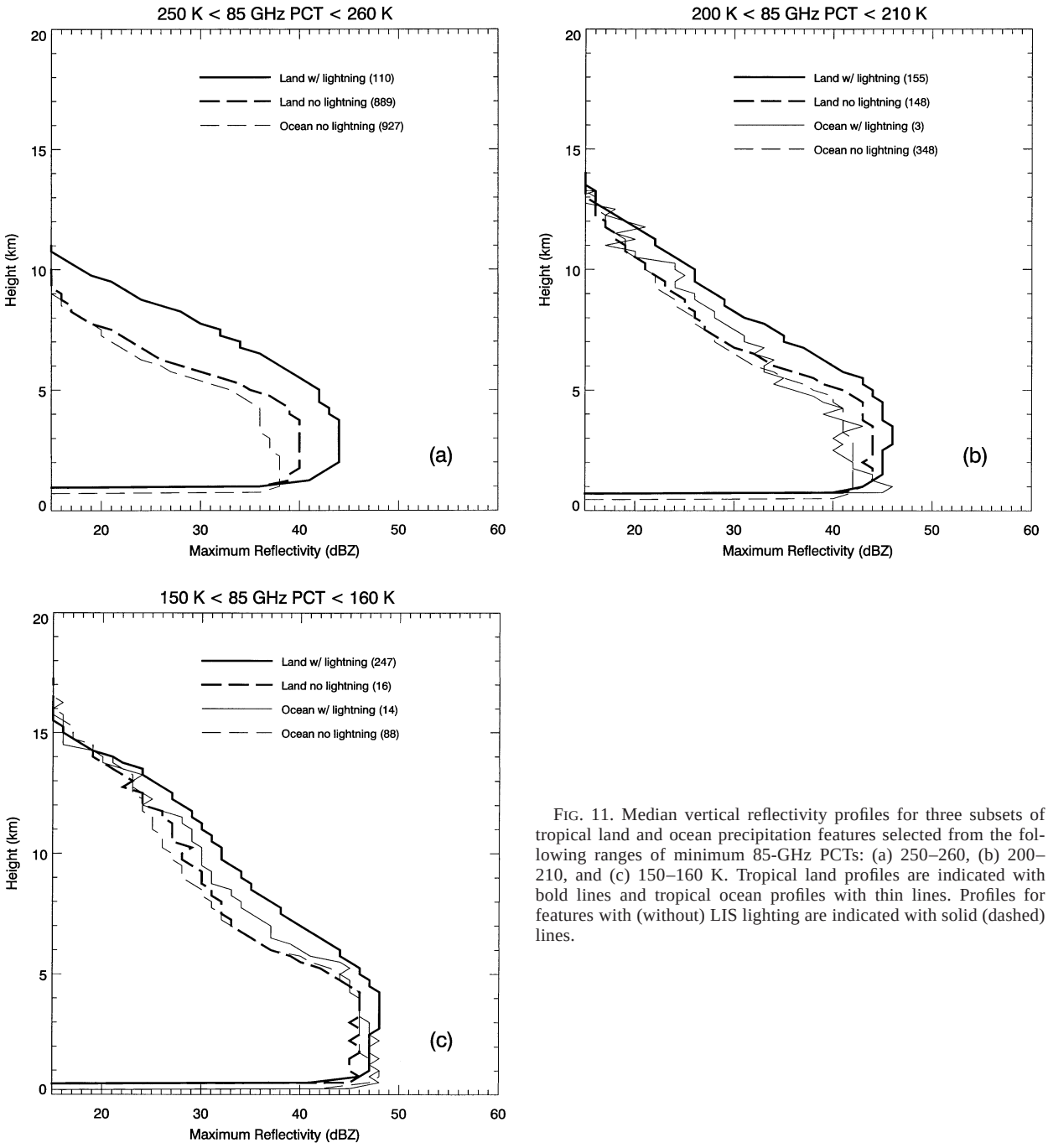

FIG. 11. Median vertical reflectivity profiles for three subsets of tropical land and ocean precipitation features selected from the following ranges of minimum 85-GHz PCTs: (a) 250–260, (b) 200–210, and (c) 150–160 K. Tropical land profiles are indicated with bold lines and tropical ocean profiles with thin lines. Profiles for features with (without) LIS lighting are indicated with solid (dashed) lines.

bilities appear more sensitive to changes in 30-dBZ heights rather than 20-dBZ heights. For instance, with the 30-dBZ echo-top height fixed at 7–8 km, the fraction of tropical continental systems with LIS lightning increases from 12% to 52% as the 20-dBZ echo increases from 7 to 12 km. With 20-dBZ heights fixed at 12–13 km, the lightning probability increases from 16% to 93% as the 30-dBZ depth increases from 6 to 11 km.

In contrast to land, the probabilities of LIS-detected lightning over the tropical oceans are near zero for systems with 30-dBZ heights below 7 km and are generally less than 25% for features with deeper 30-dBZ reflectivity. Figure 10b also indicates very clearly that tropical land systems consistently have much greater lightning probabilities than tropical ocean features with the *same reflectivity heights.* The land–ocean lightning probability differences are roughly an order of magnitude in much of the parameter space and decrease toward the reflectivity height extremes.

Figure 11 presents a comparison of the median ver-

TABLE 4. Sample sizes and LIS lightning statistics for three subsets of precipitation features selected by the minimum 85-GHz PCT.

	250 K ≤ 85-GHz PCT < 260 K			200 K ≤ 85-GHz PCT < 210 K			150 K ≤ 85-GHz PCT < 160 K		
Region	Total	Percent with lightning	Flash total	Total	Percent with lightning	Flash total	Total	Percent with lightning	Flash total
Africa	555	12	113	207	63	521	142	92	1386
South America	444	10	83	196	64	485	111	95	1393
Land	999	11	196	403	63	1006	253	94	2789
West Pacific	547	0	0	242	1	4	70	10	21
East Pacific	380	0	0	109	0	0	32	22	35
Ocean	927	0	0	351	<1	4	102	14	56

tical reflectivity structures of tropical continental and tropical oceanic systems with and without LIS lightning that have similar 85-GHz ice scattering signatures. Table 4 lists the corresponding sample sizes and LIS lightning statistics. In each 85-GHz PCT range, the tropical continental lightning profile has the greatest reflectivity values and smallest decreases in reflectivity with height (reflectivity lapse rate). At the higher T_b range (250–260 K; Fig. 11a), the reflectivity difference for land systems with and without LIS lightning is 10 dB*Z* or greater above the freezing level (~5 km). For the lower 85-GHz PCT intervals, the difference is typically 4–7 dB*Z*. In each T_b interval, the reflectivity lapse rates above the freezing level are approximately 4 dB*Z* km^{-1} for tropical continental lightning features and 5–6 dB*Z* km^{-1} for the features without lightning. Tropical land and ocean systems without LIS lightning have very similar reflectivity profiles above the freezing level in each 85-GHz PCT interval.

The reflectivity lapse rates are similar for the tropical continental and tropical oceanic lightning features in Fig. 11c, with slightly (2–4 dB*Z*) weaker reflectivity values for the tropical oceanic cases. It is also notable that the median profiles in Figs. 11b and 11c converge to similar 20-dB*Z* echo-top heights. This is indicative of the 85-GHz ice scattering response to ice particles in the upper cloud levels and it suggests that the total reflectivity depth of strong convective systems alone is not a good discriminator between tropical continental and tropical oceanic systems with or without LIS lightning.

e. Microwave signatures and LIS lightning flash rate

Figure 12 presents distributions of precipitation feature flash rates relative to the minimum 85-GHz PCT and maximum 7-km reflectivity. Figure 13 shows similar distributions using the minimum 37-GHz PCT. The 7-km level was chosen since it corresponds to a temperature range (−10° to −15°C) within the mixed phase region.

The lightning flash rates for the tropical continental features tend to increase with decreasing 85-GHz PCT and increasing 7-km reflectivity (Figs. 12a,b). The relationship is similar for 37 GHz (Figs. 13a,b), with the flash rates increasing significantly as the 37-GHz PCT decreases below about 255 K. The peak storm flash rates are 367 min^{-1} for Africa and 221 min^{-1} for South America. Not surprisingly, the majority of tropical oceanic features with LIS lightning have relatively low flash rates (Fig. 12c); the peak ocean flash rate is 26 min^{-1}.

Over land, the high flash rate features typically have 7-km reflectivities greater than about 45 dB*Z*, 85-GHz PCT < 130 K, and 37-GHz PCT < 220 K with the greatest frequency of these systems in Africa. The bulk of the tropical continental and tropical oceanic features *without* detectable lightning have 7-km reflectivities <20 dB*Z* and 85-GHz PCT > 250 K (Figs. 14a,b) or 37-GHz PCT > 260 K (Figs. 15a,b). The small fraction of systems over land and ocean without lightning and having 7-km reflectivities greater than 20 dB*Z* tend to overlap with nonzero flash rate features in their respective regions. This again suggests that at least some of the features without lightning may have nonzero flash rates that are below the LIS minimum detection level.

4. Discussion

Comparisons of the radar reflectivity echo-top height distributions for tropical oceanic and tropical continental precipitation features indicate relatively small differences in the overall echo depths (maximum 20-dB*Z* heights). Tropical land and ocean features extend to similar heights with land features reaching the extreme heights with slightly greater frequency than tropical oceanic features. There are more significant differences in relative system intensity as measured by the heights of the higher reflectivity thresholds (see Figs. 3a,b). For a given maximum 20-dB*Z* echo-top height, features over land typically have 30- and 40-dB*Z* echo-top heights that extend several kilometers higher than those in tropical oceanic systems. In addition, nearly one-third of the tropical oceanic features contain no 40-dB*Z* echo. The differences in reflectivity structure indicate that tropical continental precipitation features are typically more capable of lofting larger hydrometeors (including supercooled rain, frozen drops, and millimeter-sized graupel) to higher altitudes than most tropical oceanic features. Others have also documented substantial differences between the reflectivity structures of tropical continental

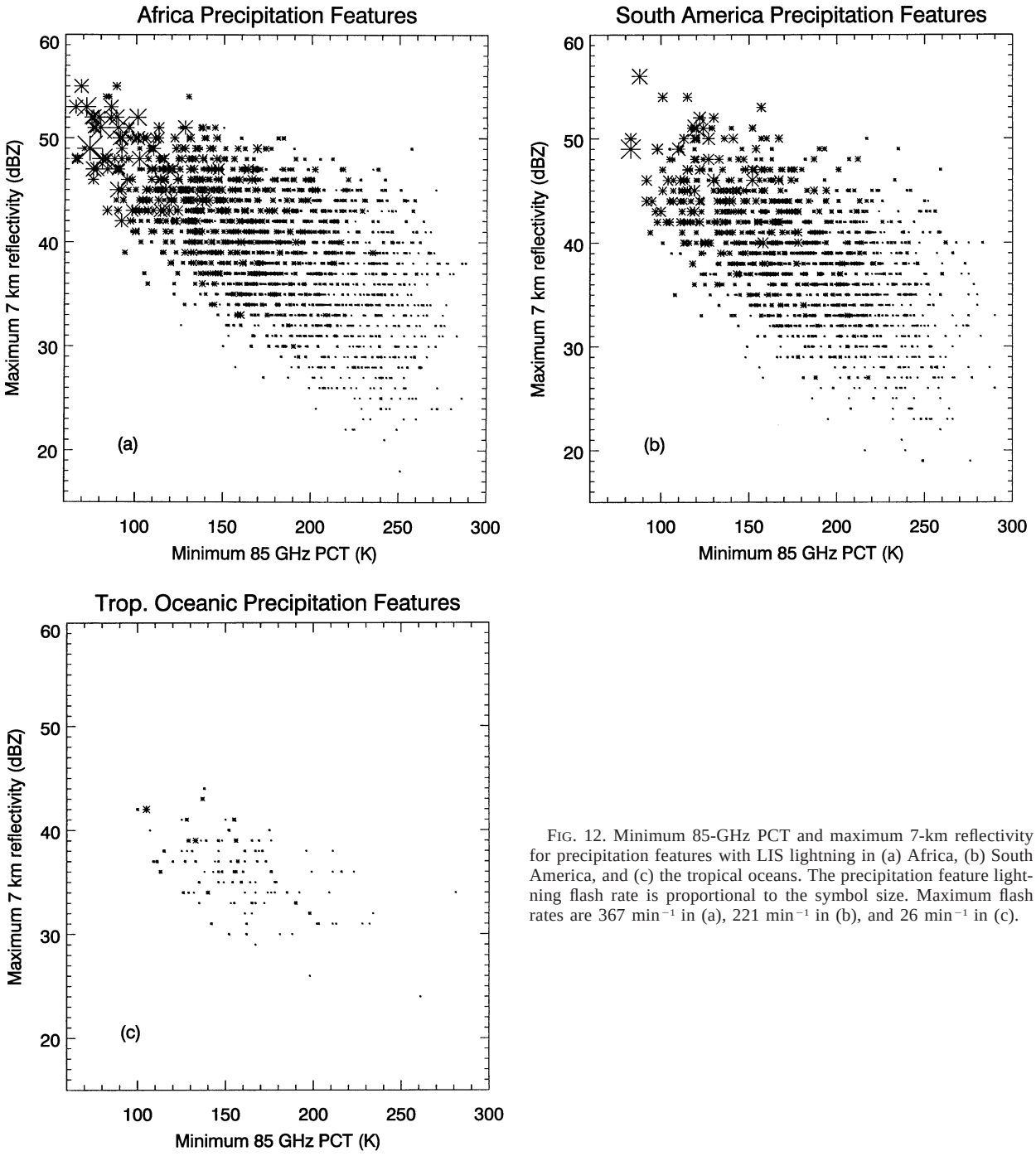

FIG. 12. Minimum 85-GHz PCT and maximum 7-km reflectivity for precipitation features with LIS lightning in (a) Africa, (b) South America, and (c) the tropical oceans. The precipitation feature lightning flash rate is proportional to the symbol size. Maximum flash rates are 367 min^{-1} in (a), 221 min^{-1} in (b), and 26 min^{-1} in (c).

and tropical oceanic storms (Rutledge et al. 1992; Williams et al. 1992; Zipser and Lutz 1994). These findings are consistent with well-documented characteristically weak updraft magnitudes of tropical oceanic storms (Zipser and LeMone 1980; Jorgensen and LeMone 1989; Lucas et al. 1994).

The relatively weak tropical oceanic updrafts have a twofold effect in terms of the observed reflectivity structure. First, the bulk of the hydrometeor mass falls out without being carried sufficiently above the freezing level to grow by accretion processes. Second, the weak updrafts limit the supply of supercooled liquid water in the mixed phase portion of the cloud such that the many small hydrometeors are competing for the available supercooled liquid water. Jorgensen et al. (1985) find that sharp reflectivity decreases above the freezing level in hurricane updrafts are coincident with decreases in the amount of supercooled liquid water above that level,

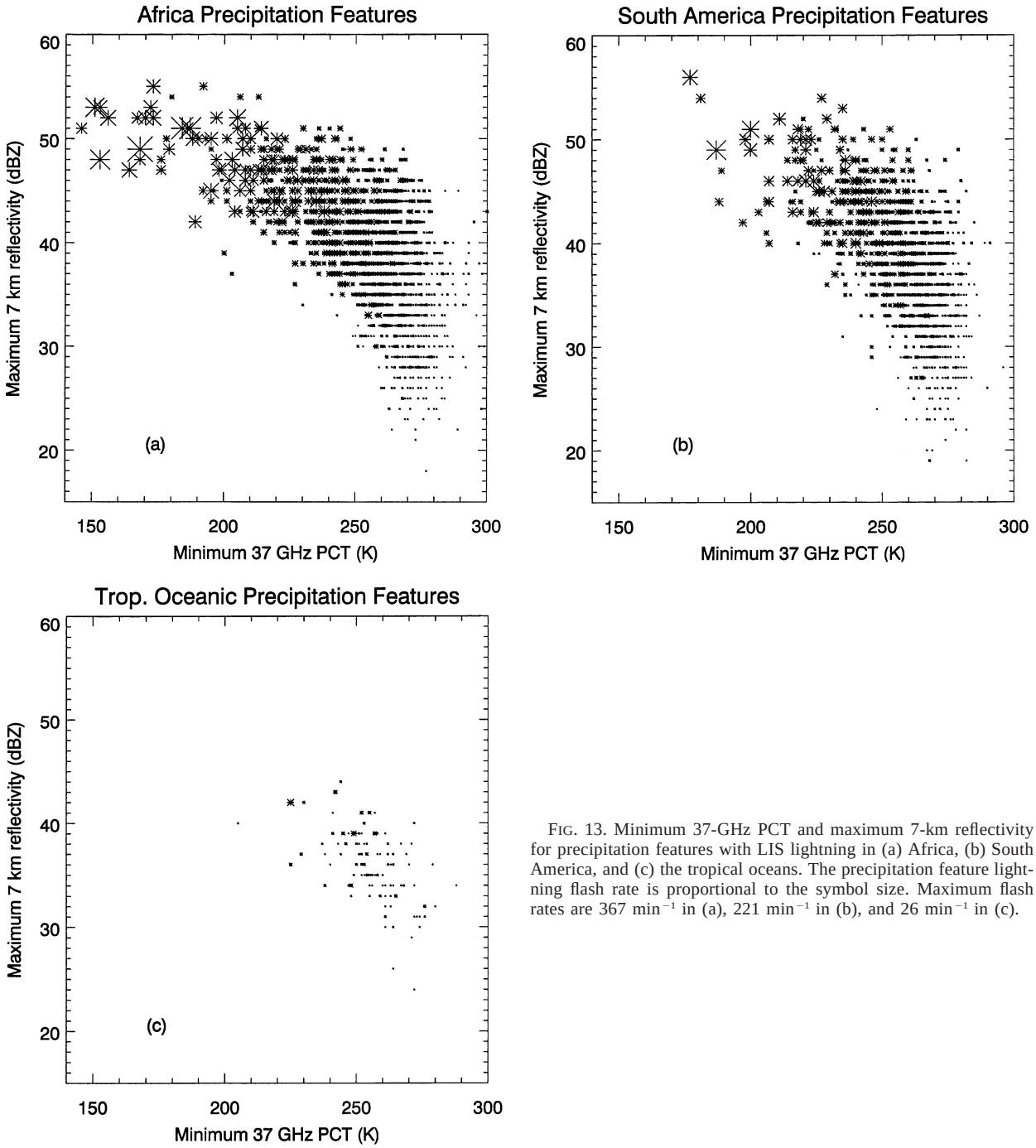

FIG. 13. Minimum 37-GHz PCT and maximum 7-km reflectivity for precipitation features with LIS lightning in (a) Africa, (b) South America, and (c) the tropical oceans. The precipitation feature lightning flash rate is proportional to the symbol size. Maximum flash rates are 367 min^{-1} in (a), 221 min^{-1} in (b), and 26 min^{-1} in (c).

which limits the potential for particle growth, and they attribute this to the observed weak updrafts.

The observed reflectivity differences between tropical continental and tropical oceanic precipitation features are consistent, at least in a bulk sense, with the distributions of minimum 85- and 37-GHz brightness temperatures. One obvious difference between land and ocean systems is the fact that tropical continental features reach lower 85- and 37-GHz brightness temperature extremes than tropical oceanic features (Fig. 3c). This result is not particularly unique as the land bias in 85-GHz ice scattering intensity has been previously documented (Mohr and Zipser 1996; Zolman et al. 2000; Nesbitt et al. 2000). However, a more subtle but nonetheless important finding is that features over land typically have lower 37-GHz PCTs for a given 85-GHz PCT than oceanic features, particularly where appreciable 85-GHz ice scattering is indicated (PCT $<$ 250 K).

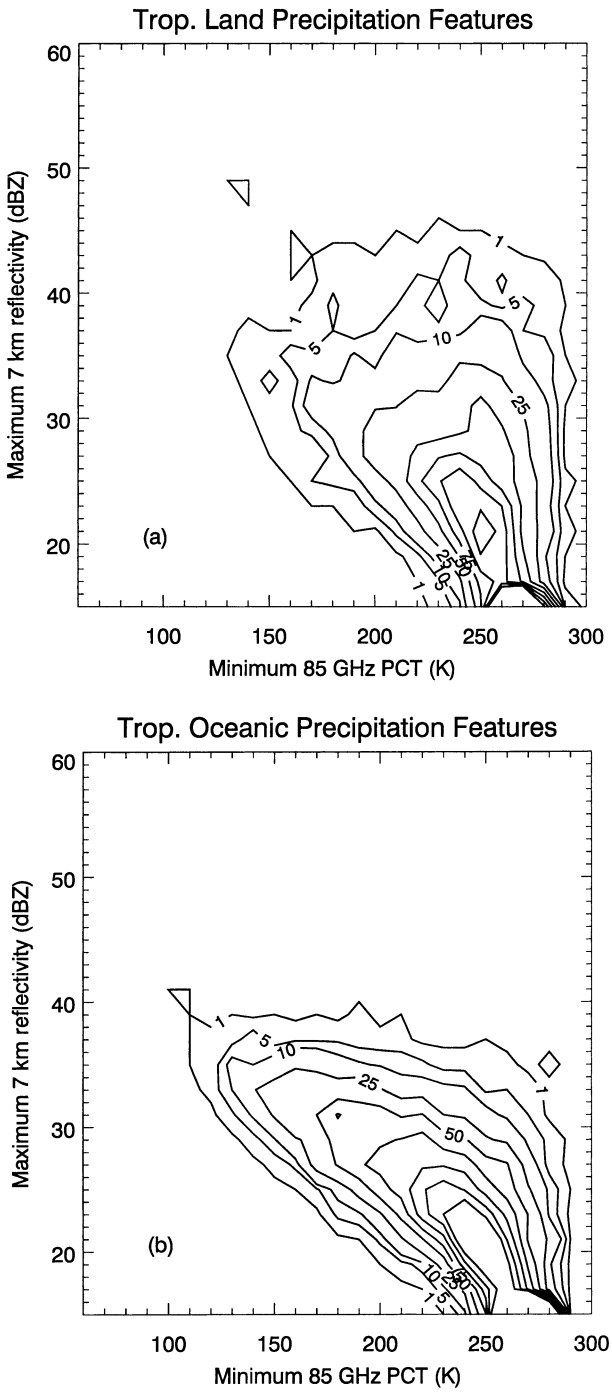

FIG. 14. Frequency distribution of (a) tropical continental and (b) tropical oceanic precipitation features without LIS lightning as a function of minimum 85-GHz PCT and maximum 7-km reflectivity. Bin size is 2 dBZ for ordinate and 10 K for the abscissa. Bin labels represent the lower value of the bin range. Contour values are 1, 5, 10, 25, 50, 75, 100, 125, and 150.

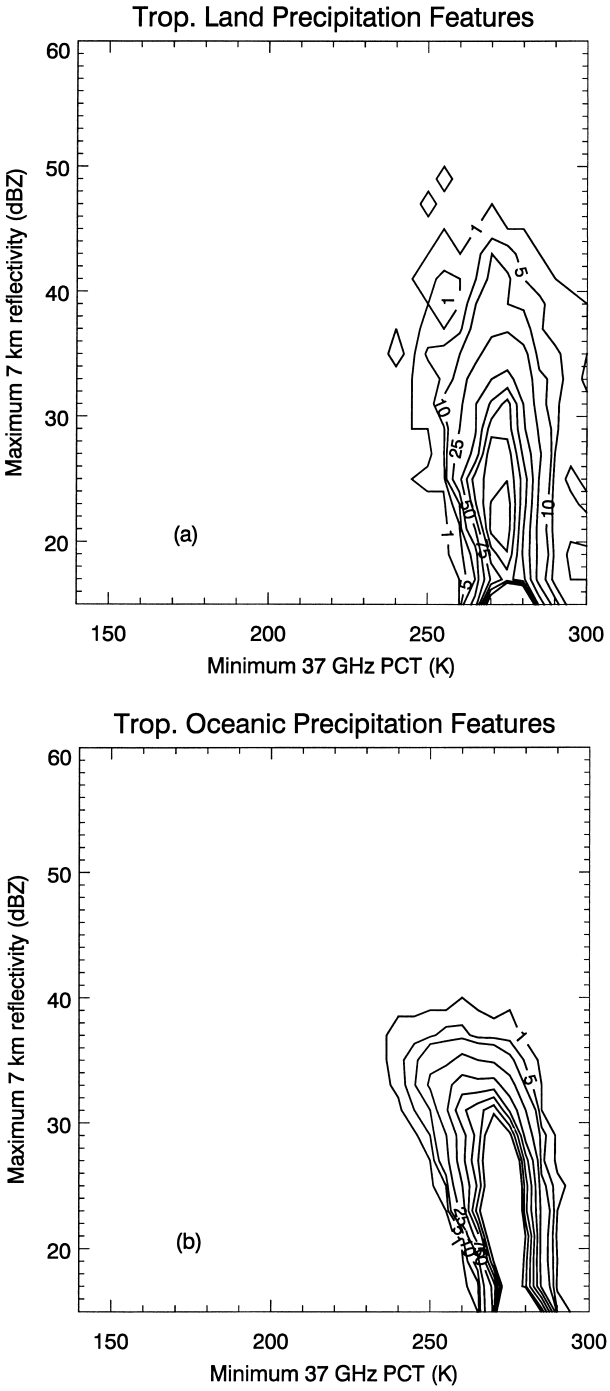

FIG. 15. Frequency distribution of (a) tropical continental and (b) tropical oceanic precipitation features without LIS lightning as a function of minimum 37-GHz PCT and maximum 7-km reflectivity. Bin size is 2 dBZ for ordinate and 5 K for the abscissa. Bin labels represent the lower value of the bin range. Contour values are 1, 5, 10, 25, 50, 75, 100, 125, and 150.

Thus, for a given degree of significant 85-GHz ice scattering, the 37-GHz frequency responds to the larger graupel or hail particles more likely to be present in the tropical continental features. This is corroborated by the observed differences in the 30- and 40-dBZ echo-top heights between tropical oceanic and tropical continental storms indicating that the larger graupel or hail particles are more likely to occur and extend to higher altitudes in the continental cases.

A complementary explanation for the observation that tropical land systems have lower 37-GHz PCTs than tropical oceanic systems with the same 85-GHz ice scattering signatures is that the land systems may contain a greater concentration of supercooled cloud liquid water aloft than their oceanic counterparts. Several modeling studies have demonstrated that the presence of cloud liquid water above the freezing level acts as an emission source that can partially mask the effects of 85-GHz ice scattering on upwelling radiation (Alder et al. 1991; Vivekanandan et al. 1991; Smith et al. 1992; Seo 2000). The net result is that the computed 85-GHz brightness temperatures are warmer than would otherwise be observed. Thus, the presence of large graupel aloft in the tropical continental systems would contribute to the lower 37-GHz PCTs (relative to the ocean systems), while at the same time at 85 GHz, the competing effects of ice scattering and emission from supercooled liquid water constrain the 85-GHz PCTs.

Tropical continental features typically have warmer 85-GHz PCTs than tropical oceanic features when normalized by the radar echo-top heights. The brightness temperature differences between tropical oceanic and tropical continental systems are usually 5–15 K across much of the echo-top height parameter space, particularly where the minimum 85-GHz PCTs are below 250 K indicating significant 85-GHz ice scattering. Such a consistent relationship is difficult to explain unless one considers the effect of supercooled cloud liquid water on the measured 85-GHz brightness temperatures. Since the cloud water droplets are too small to contribute to reflectivity at the PR wavelength, it is reasonable to infer that a greater supercooled liquid water content aloft in the tropical continental systems would yield higher 85-GHz T_b than tropical ocean systems with similar reflectivity heights.

When normalized by the 37-GHz brightness temperatures, particularly where significant 37-GHz ice scattering is occurring (PCT $<$ 255 K), tropical land systems extend to much higher 85-GHz brightness temperatures than the tropical oceanic systems. The higher 85-GHz T_bs may be indicative of a smaller optical depth at this frequency, which can result from a shallower layer of ice aloft, the presence of lower density ice particles, a smaller concentration of scatterers, or combinations of these factors. Here again we also suggest that it is possible for the higher 85-GHz PCTs to be related to the presence of greater supercooled cloud liquid water contents in the mixed phase regions of these land systems. The 37-GHz ice scattering signature suggests that the tropical land and ocean systems have sufficient quantities of cloud liquid water above the freezing level to grow large graupel. However, cloud liquid water may extend through a deeper vertical layer and in greater quantities in the land systems.

The relationships between reflectivity, brightness temperatures, and lightning (as detected by LIS) for the tropical continental and tropical oceanic features reveal robust trends that can be at least partly understood in terms of cloud microphysics. For instance, the lightning flash rates generally increase with decreasing 85- and 37-GHz PCTs and increasing 7-km reflectivity. The 7-km level ($-10°$ to $-15°$C) is within the mixed phase region where noninductive charge separation would likely occur (Takahashi 1978; Jayaratne et al. 1983; Williams 1989; Saunders et al. 1991). Observations of midlatitude thunderstorms (Dye et al. 1986, 1989), tropical island convection (Carey and Rutledge 2000), and tropical oceanic convection (Petersen et al. 1996) show that rapid cloud electrification occurs with the presence of millimeter-sized graupel or frozen drops and high reflectivity (35–40 dBZ) above 6–7 km. The relationship between flash rate and the 85- and 37-GHz PCTs is consistent with the response of the microwave frequencies to an increase in the number and size of liquid and frozen particles in the mixed phase region of the storm, which is conducive to vigorous charge separation.

It was noted that it is possible for a tropical continental feature to have LIS-detected lightning almost without regard to the 85- or 37-GHz brightness temperatures, while tropical oceanic features have a near-zero lightning probability (or are weakly electrified) without significant 85-GHz ice scattering (PCT $<$ 180 K) occurring. Also, tropical continental features consistently show much greater lightning probabilities than tropical oceanic features with very similar brightness temperatures (Fig. 10a) or very similar reflectivity heights (Fig. 10b). Interpretation of these results must include consideration of the limitations imposed by the LIS minimum detectable flash rate ($\sim$1 min^{-1}). It is highly likely that a significant fraction of systems in our sample have nonzero flash rates that are below the LIS minimum detectable flash rate. Thus, it is highly likely that the limitations of LIS explain at least some of the differences in lightning probability between land and ocean systems that are normalized by reflectivity height or brightness temperature. However, this large sample of data shows significantly different flash rates for land and ocean systems with similar reflectivity heights or brightness temperatures, suggesting the existence of physical or microphysical differences that should be explored.

One possible partial explanation for the lightning probability differences between land and ocean systems with similar reflectivity heights, apart from microphysical differences, is related to convective area. That is, one would expect the probability of lightning to have

some relationship to the size and/or number of convective cores (i.e., area of deep reflectivity) in a system. However, at best, any such difference in the size or number of convective cores would only *contribute* to the land–ocean difference in lightning probability. Land and ocean systems with similar numbers and/or sizes of convective cores do have very different lightning characteristics.

The lightning probability differences for tropical continental and tropical oceanic storms with similar brightness temperatures can be at least partially understood by considering that the magnitude of ice scattering is largely determined by the characteristics of the ice layer. Similar brightness temperatures can result from ice layers with quite different depths, ice particle densities, size distributions, shapes, and number densities. The characteristics of the ice layer that give similar brightness temperatures may be conducive to charge separation in one system but not in another. The concentration and vertical distribution of supercooled liquid water may also be a factor. For instance, a convective cloud with enhanced 85-GHz ice scattering by large graupel that is offset by emission from enhanced supercooled liquid water may yield the same brightness temperature but much more charge separation than a convective cloud with smaller (or less) ice and less supercooled liquid water.

The vertical profiles of reflectivity provide additional information to the lightning probability–brightness temperature relationships. For the same degree of 85-GHz ice scattering, continental features with lightning tend to have greater reflectivity values and smaller decreases of reflectivity with height above the freezing level than ocean features with lightning. Features without lightning, whether tropical continental or oceanic, are characterized by the weakest vertical reflectivity profiles. These relationships can be interpreted in terms of the cloud liquid water content supplied to the mixed phase regions of these systems, which is largely governed by updraft velocity and the number of cloud condensation nuclei (CCN) available. It is well known that maritime air masses contain far fewer CCN concentrations than continental air masses (Pruppacher and Klett 1997). For the ocean clouds, this translates to a greater precipitation efficiency, a shorter residence time for cloud water droplets, and a lower cloud liquid water content than continental clouds for a given vertical velocity. In contrast, greater numbers of CCN in continental clouds result in a greater number of small cloud droplets, an inefficient coalescence process, longer cloud droplet residence time, and greater cloud liquid water content.

Stronger updrafts will also result in a greater cloud liquid water content supplied to the mixed phase region of the cloud. The supercooled water contributes to graupel growth through accretion and is a critical component of robust charge separation via the noninductive ice–ice collision mechanism. While the supercooled cloud droplets are not contributing to the reflectivity signature, larger (millimeter sized) supercooled raindrops, sustained aloft by the updrafts, are highly reflective and together with the growing graupel yield larger reflectivity values above the freezing level and smaller decreases of reflectivity with height than in systems without lightning. While we have no direct information about updraft velocities in this dataset, the fact that a small fraction of tropical oceanic systems have lightning suggests that these systems have updraft magnitudes vigorous enough to supply sufficient supercooled liquid water to the mixed phase region for robust charge separation to occur. However, these processes are much more efficient in the tropical continental lightning features.

The vast disparity in tropical continental and tropical oceanic lightning flash densities results from both the increased likelihood of lightning occurring in tropical continental storms *and* the extreme flash rates produced by the most intense storms, found almost exclusively in continental regimes. Boccippio et al. (2000) show that the mean flash rates for lightning producing storms are only about a factor of 2 greater for tropical continental storms than for tropical oceanic storms. The arithmetic mean, however, is dominated by the many low flash rate storms. The extreme flash rates are an order of magnitude greater, and are more common, in tropical continental precipitation features than in tropical oceanic precipitation features.

Most of the precipitation features over Africa and South America have similar reflectivity signatures, 85- and 37-GHz signatures, and lightning flash rates. However, Africa tends to have a greater occurrence of intense features at the low brightness temperature and high reflectivity extremes, which often have high flash rates. The occurrence of these intense systems over Africa may account for the observed regional differences in lightning flash count and flash density.

5. Summary and conclusions

The bulk radar reflectivity structures and passive microwave 85- and 37-GHz brightness temperature signatures are presented for a large sample of tropical continental and tropical oceanic precipitation features with and without LIS-detected lightning from four regions in the Tropics: Africa, South America, east Pacific, and west Pacific. The dataset is that used by Nesbitt et al. (2000) who define a precipitation feature as a contiguous area $\geq$75 km^2 with either a near-surface reflectivity $\geq$20 dBZ or an 85-GHz PCT $\leq$ 250 K. The objective is to compare the relative strengths of the tropical land and ocean precipitation features according to the strongest convective events within the precipitation features and the relationship to lightning as observed by the LIS instrument.

The observations show that tropical continental features often have stronger vertical reflectivity profiles (i.e., larger magnitudes of reflectivity and smaller de-

creases in reflectivity with height) than tropical oceanic features. That is, for a given 20-dB*Z* echo-top height the layer of 30- and 40-dB*Z* echo is deeper in tropical continental systems than in tropical ocean systems. In fact, 30% of the tropical oceanic features have no 40-dB*Z* echo, compared with 10% of those over land. The weak tropical ocean reflectivity profiles are consistent with characteristically weak vertical velocities noted previously in tropical oceanic storms, which are insufficient to sustain large liquid or frozen hydrometeors much above the freezing level (Zipser and LeMone 1980; Jorgensen and LeMone 1989; Lucas et al. 1994).

The trends in the bulk reflectivity profiles are also consistent with the observed 85- and 37-GHz brightness temperature distributions. The tropical continents tend to have a greater fraction of precipitation features with colder brightness temperatures than the tropical ocean regions. For a given degree of 85-GHz ice scattering, the tropical continental features typically have colder minimum 37-GHz PCTs than the ocean features, indicating the presence of larger graupel or hail in the continental systems.

For a given degree of significant 37-GHz ice scattering (PCT $<$ 255 K), tropical continental and tropical oceanic features have similar modal 85-GHz signatures, with the land systems extending to much warmer 85-GHz PCTs. Also, when normalized by the radar echo-top heights, the minimum 85-GHz PCTs for tropical continental features are consistently 5–15 K warmer than the tropical oceanic features. It is inferred in both instances that the brightness temperature differences may be a result of greater cloud liquid water contents above the freezing level in the tropical continental features, which acts as an emission source to partially mask the 85-GHz ice scattering effects.

The LIS lightning distributions are strongly land biased, as other studies have shown (Orville and Hendersen 1986; Goodman and Christian 1993; and others), with flash densities differing by as much as two orders of magnitude between tropical land and ocean. When the precipitation feature lightning characteristics are considered in relation to the radar reflectivity and brightness temperature signatures, the following relationships emerge:

1) When normalized by minimum brightness temperatures, tropical continental features consistently have much higher lightning probabilities than features over the tropical oceans. It is inferred that the difference is related in part to greater supercooled liquid water contents in the continental systems.
2) When normalized by radar echo-top heights, tropical continental features consistently have much higher lightning probabilities than tropical oceanic features. Tentative hypotheses to explain the difference include greater convective area in the tropical continental features, or more efficient electrification through subtly different cloud microphysics such as greater cloud liquid water contents aloft in tropical continental systems.
3) For a given degree of 85-GHz ice scattering, features with LIS lightning have larger reflectivity values and smaller decreases of reflectivity with height above the freezing level than features without detected lightning.
4) Lightning flash rates generally increase with decreasing 85- and 37-GHz brightness temperatures and increasing midlevel reflectivity.

The interpretation of the lightning results is constrained somewhat by the LIS minimum detectable flash rate (1 min^{-1}). For instance, some of the overlap in the reflectivity height and brightness temperature parameter space between features with and without detected lightning is undoubtedly due to the LIS minimum flash rate limit. However, LIS limitations notwithstanding, some of the relationships between lightning, radar, and the ice scattering signatures of the tropical land and ocean precipitation features in this sample are consistent with what is known or hypothesized about the differences in land and ocean lightning occurrence, while others are less clear. The remotely sensed TRMM observables do not provide direct microphysics information and the inferences based on the observations are best addressed through the use of numerical cloud model and radiative transfer model techniques, in addition to coupled in situ microphysics and remote sensing observations. By the same token, the data presented here represent a quantitative observational framework that can be used to help provide constraints on cloud model input to radiative transfer models and validation for radiative transfer model results.

Acknowledgments. We would like to thank Chris West for programming assistance. We especially thank two anonymous reviewers for their constructive comments. The Lightning Imaging Sensor data were made available from the Global Hydrology Resource Center at the Global Hydrology and Climate Center, Huntsville, Alabama. The TRMM Microwave Imager and Precipitation Radar data were made available from the TRMM Science Data and Information System. This research is made possible through funding by grants from the National Aeronautics and Space Administration (NAG5-4699, NAG5-4796) as well as a NASA Earth System Science Fellowship (406027).

REFERENCES

Adler, R. F., H.-Y. M. Yeh, N. Prasad, W.-K. Tao, and J. Simpson, 1991: Microwave simulations of a tropical rainfall system with a three-dimensional cloud model. *J. Appl. Meteor.,* **30,** 924–953.

Black, R. A., and J. Hallett, 1999: Electrification of the hurricane. *J. Atmos. Sci.,* **56,** 2004–2028.

Boccippio, D. J., S. J. Goodman, and S. Heckman, 2000: Regional differences in tropical lightning distributions. *J. Appl. Meteor.,* **39,** 2231–2248.

Carey, L. D., and S. A. Rutledge, 2000: The relationship between precipitation and lightning in tropical island convection: A C-band polarimetric radar study. *Mon. Wea. Rev.,* **128,** 2687–2710.

Cecil, D. J., and E. J. Zipser, 2002: Reflectivity, ice scattering, and lightning characteristics of hurricane eyewalls and rainbands. Part II: Intercomparison of observations. *Mon. Wea. Rev.,* **130,** 785–801.

——, ——, and S. W. Nesbitt, 2002: Reflectivity, ice scattering, and lightning characteristics of hurricane eyewalls and rainbands. Part I: Quantitative description. *Mon. Wea. Rev.,* **130,** 769–784.

Christian, H. J., 1999. *Atmospheric Electricity,* Guntersville, AL, NASA/CP-1999-209261, 715–718.

——, and Coauthors, 1999: Global frequency and distribution of lightning as observed by the Optical Transient Detector (OTD). *Proc. 11th Int. Conf. on Atmospheric Electricity,* Guntersville, AL, NASA/CP-1999-209261, 726–729.

Dye, J. E., and Coauthors, 1986: Early electrification and precipitation development in a small, isolated Montana cumulonimbus. *J. Geophys. Res.,* **91,** 1231–1247.

——, W. P. Winn, J. J. Jones, and D. W. Breed, 1989: The electrification of New Mexico thunderstorms 1. Relationship between precipitation development and the onset of electrification. *J. Geophys. Res.,* **94,** 8463–8656.

Ferraro, R. R., N. C. Grody, and G. F. Marks, 1994: Effects of surface conditions on rain identification using the DMSP-SSM/I. *Remote Sens. Rev.,* **11,** 195–209.

Fulton, R., and G. M. Heymsfield, 1991: Microphysical and radiative characteristics of convective clouds during COHMEX. *J. Appl. Meteor.,* **30,** 98–116.

Goodman, S. J., and H. Christian, 1993: Global observations of lightning. *Atlas of Satellite Observations Related to Global Change,* R. J. Gurney, J. L. Foster, and C. L. Parkinson, Eds., Cambridge University Press, 191–219.

Grody, N. C., 1991: Classification of snow cover and precipitation using the Special Sensor Microwave/Imager. *J. Geophys. Res.,* **96,** 7423–7435.

Hakkarinen, I. M., and R. F. Adler, 1988: Observations of precipitating convective systems at 92 and 183 GHz: Aircraft results. *Meteor. Atmos. Phys.,* **38,** 164–182.

Heymsfield, G. M., and R. Fulton, 1988: Comparison of high-altitude remote aircraft measurements with the radar structure of an Oklahoma thunderstorm: Implications for precipitation estimation from space. *Mon. Wea. Rev.,* **116,** 1157–1174.

——, and ——, 1994: Passive microwave and infrared structure of mesoscale convective systems. *Meteor. Atmos. Phys.,* **54,** 123–139.

Jayaratne, E. R., C. P. R. Saunders, and J. Hallett, 1983: Laboratory studies of the charging of soft-hail during ice crystal interactions. *Quart. J. Roy. Meteor. Soc.,* **109,** 609–630.

Jorgensen, D. P., and M. A. LeMone, 1989: Vertical velocity characteristics of oceanic convection. *J. Atmos. Sci.,* **46,** 621–640.

——, E. J. Zipser, and M. A. LeMone, 1985: Vertical motions in intense hurricanes. *J. Atmos. Sci.,* **42,** 839–856.

Keighton, S. J., H. B. Bluestein, and D. R. MacGorman, 1991: The evolution of a severe mesoscale convective system: Cloud-to-ground lightning location and storm structure. *Mon. Wea. Rev.,* **119,** 1533–1556.

Kummerow, C., 1993: On the Eddington approximation for radiative transfer in the microwave frequencies. *J. Geophys. Res.,* **98,** 2757–2765.

——, W. Barnes, T. Kozu, J. Shiue, and J. Simpson, 1998: The Tropical Rainfall Measuring Mission (TRMM) sensor package. *J. Atmos. Oceanic Technol.,* **15,** 809–817.

Lucas, C., E. J. Zipser, and M. A. LeMone, 1994: Vertical velocity in oceanic convection off tropical Australia. *J. Atmos. Sci.,* **51,** 3183–3193.

Mohr, K. I., and E. J. Zipser, 1996: Defining mesoscale convective systems by the 85-GHz ice scattering signatures. *Bull. Amer. Meteor. Soc.,* **77,** 1179–1188.

——, E. R. Toracinta, E. J. Zipser, and R. E. Orville, 1996: A comparison of WSR-88D reflectivities, SSM/I brightness temperatures, and lightning for mesoscale convective systems in Texas. Part II: SSM/I brightness temperatures and lightning. *J. Appl. Meteor.,* **35,** 919–931.

——, J. S. Famiglietti, and E. J. Zipser, 1999: The contribution to tropical rainfall with respect to convective system type, size, and intensity estimated from the 85-GHz ice-scattering signature. *J. Appl. Meteor.,* **38,** 596–606.

Mugnai, A., H. J. Cooper, E. A. Smith, and G. J. Tripoli, 1990: Simulation of microwave brightness temperatures of an evolving hailstorm at SSM/I frequencies. *Bull. Amer. Meteor. Soc.,* **71,** 2–13.

Nesbitt, S. W., E. J. Zipser, and D. J. Cecil, 2000: A census of precipitation features in the Tropics using TRMM: Radar, ice scattering, and lightning observations. *J. Climate,* **13,** 4087–4106.

Orville, R. E., and R. Henderson, 1986: Global distribution of midnight lightning: September 1977 to August 1978. *Mon. Wea. Rev.,* **114,** 2640–2653.

Petersen, W. A., and S. A. Rutledge, 2001: Regional variability in tropical convection: Observations from TRMM. *J. Climate,* **14,** 3566–3586.

——, ——, and R. E. Orville, 1996: Cloud-to-ground lightning observations from TOGA COARE: Selected results and lightning location algorithms. *Mon. Wea. Rev.,* **124,** 602–620.

——, R. C. Cifelli, S. A. Rutledge, B. S. Ferrier, and B. F. Smull, 1999: Shipborne dual-Doppler operations during TOGA COARE: Integrated observations of storm kinematics and electrification. *Bull. Amer. Meteor. Soc.,* **80,** 81–97.

Pruppacher, H. R., and J. D. Klett, 1997: *Microphysics of Clouds and Precipitation.* 2d ed. Kluwer Academic, 954 pp.

Reynolds, S. E., M. Brook, and M. F. Gourley, 1957: Thunderstorm charge separation. *J. Meteor.,* **14,** 426–436.

Riehl, H., 1954: *Tropical Meteorology.* McGraw-Hill, 392 pp.

Rutledge, S. A., and D. R. MacGorman, 1988: Cloud-to-ground lightning activity in the 10–11 June 1985 mesoscale convective system observed during the Oklahoma–Kansas PRE-STORM Project. *Mon. Wea. Rev.,* **116,** 1393–1408.

——, E. R. Williams, and T. D. Keenan, 1992: The Down under Doppler and Electricity Experiment (DUNDEE): Overview and preliminary results. *Bull. Amer. Meteor. Soc.,* **73,** 3–16.

Saunders, C. P. R., W. D. Keith, and R. P. Mitzeva, 1991: The effect of liquid water on thunderstorm charging. *J. Geophys. Res.,* **96,** 11 007–11 017.

Seo, E.-K., 2000: Sensitivity of hydrometeor profiles and satellite brightness temperatures to model microphysics for MCSs over land and ocean: Model comparison using EOF analysis and implications for rain and latent heat retrievals. Ph.D. dissertation, Texas A&M University, 177 pp.

Simpson, J., R. F. Adler, and G. R. North, 1986: On the Tropical Rainfall Measuring Mission (TRMM). *Meteor. Atmos. Phys.,* **60,** 19–36.

Smith, E. A., A. Mugnai, H. J. Cooper, G. J. Tripoli, and X. Xiang, 1992: Foundations for statistical physical precipitation retrieval from passive microwave satellite measurements. Part I: Brightness temperature properties of a time-dependent cloud radiation model. *J. Appl. Meteor.,* **31,** 506–531.

Spencer, R. W., 1986. A satellite passive 37-GHz scattering-based method for measuring oceanic rain rates. *J. Climate Appl. Meteor.,* **27,** 754–766.

——, H. M. Goodman, and R. E. Hood, 1989: Precipitation retrieval over land and ocean with the SSM/I: Identification and characteristics of the scattering signal. *J. Atmos. Oceanic Technol.,* **6,** 254–273.

Takahashi, T., 1978: Riming electrification as a charge generation mechanism in thunderstorms. *J. Atmos. Sci.,* **35,** 1536–1548.

Toracinta, E. R., and E. J. Zipser, 2001: Lightning and SSM/I ice scattering mesoscale convective systems in the global Tropics. *J. Appl. Meteor.,* **40,** 983–1002.

——, K. I. Mohr, E. J. Zipser, and R. E. Orville, 1996: A comparison of WSR-88D reflectivities, SSM/I brightness temperatures, and

lightning for mesoscale convective systems in Texas. Part I: Radar reflectivity and lightning. *J. Appl. Meteor.,* **35,** 902–918.
Vivekanandan, J., J. Turk, G. L. Stephens, and V. N. Bringi, 1990: Microwave radiative transfer studies using combined multiparameter radar and radiometer measurements during COHMEX. *J. Appl. Meteor.,* **29,** 561–585.
——, ——, and V. N. Bringi, 1991: Ice water path estimation and characterization using passive microwave radiometery. *J. Appl. Meteor.,* **30,** 1407–1421.
Wilheit, T. T., 1986: Some comments on passive microwave measurement of rain. *Bull. Amer. Meteor. Soc.,* **67,** 1226–1232.
——, and Coauthors, 1982: Microwave radiometric observations near 19.35, 92, and 183 GHz of precipitation in Tropical Storm Cora. *J. Appl. Meteor.,* **21,** 1137–1145.
Williams, E. R., 1989: The tripole structure of thunderstorms. *J. Geophys. Res.,* **94,** 13 151–13 167.
——, S. A. Rutledge, S. G. Geotis, N. Renno, E. Rasmussen, and T. Rickenback, 1992: A radar and electrical study of tropical ''hot towers.'' *J. Atmos. Sci.,* **49,** 1386–1395.
——, K. Rothkin, D. Stevenson, and D. J. Boccippio, 2000: Global lightning variability caused by changes in thunderstorm flash rate and by changes in number of thunderstorms. *J. Appl. Meteor.,* **39,** 2223–2230.
Wu, R., and J. A. Weinman, 1984: Microwave radiances from precipitating clouds containing aspherical ice, combined phase, and liquid hydrometeors. *J. Geophys. Res.,* **89,** 7170–7178.
Zipser, E. J., 1994: Deep cumulonimbus cloud systems in the Tropics with and without lightning. *Mon. Wea. Rev.,* **122,** 1837–1851.
——, and M. A. LeMone, 1980: Cumulonimbus vertical velocity events in GATE. Part II: Synthesis and model core structure. *J. Atmos. Sci.,* **37,** 2458–2469.
——, and K. R. Lutz, 1994: The vertical profile of radar reflectivity of convective cells: A strong indicator of storm intensity and lightning probability. *Mon. Wea. Rev.,* **122,** 1751–1759.
Zolman, J. L., E. J. Zipser, and K. I. Mohr, 2000: A comparison of tropical mesoscale convective systems in El Niño and La Niña. *J. Climate,* **13,** 3314–3326.